J|A|C|S ARTICLES

Published on Web 05/04/2010

Membrane-Bound Hydrogenase I from the Hyperthermophilic Bacterium *Aquifex aeolicus*: Enzyme Activation, Redox Intermediates and Oxygen Tolerance

Maria-Eirini Pandelia,[†,‡] Vincent Fourmond,[‡,§] Pascale Tron-Infossi,[§] Elisabeth Lojou,[§] Patrick Bertrand,[§] Christophe Léger,[§] Marie-Thérèse Giudici-Orticoni,[§] and Wolfgang Lubitz[†,*]

Max-Planck-Institut für Bioanorganische Chemie, Stiftstrasse 34-36, D45470, Mülheim a.d. Ruhr, Germany, and CNRS UPR 9036, Institut de Biologie de la Méditerranée, 31 chemin Joseph Aiguier, 13402 Marseille Cedex 20, France

Received December 23, 2009; E-mail: lubitz@mpi-muelheim.mpg.de

Abstract: The membrane-bound hydrogenase (Hase I) of the hyperthermophilic bacterium *Aquifex aeolicus* belongs to an intriguing class of redox enzymes that show enhanced thermostability and oxygen tolerance. Protein film electrochemistry is employed here to portray the interaction of Hase I with molecular oxygen and obtain an overall picture of the catalytic activity. Fourier transform infrared (FTIR) spectroscopy integrated with *in situ* electrochemistry is used to identify structural details of the [NiFe] site and the intermediate states involved in its redox chemistry. We found that the active site coordination is similar to that of standard hydrogenases, with a conserved $Fe(CN)_2CO$ moiety. However, only four catalytic intermediates could be detected; these correspond structurally to the Ni-B, Ni-SI_a, Ni-C, and Ni-R states of standard hydrogenases. The Ni-SI/Ni-C and Ni-C/Ni-R midpoint potentials are approximately 100 mV more positive than those observed in mesophilic hydrogenases, which may be the reason that *A. aeolicus* Hase I is more suitable as a catalyst for H_2 oxidation than production. Protein film electrochemistry shows that oxygen inhibits the enzyme by reacting at the active site to form a single species (Ni-B); the same inactive state is obtained under oxidizing, anaerobic conditions. The mechanism of anaerobic inactivation and reactivation in *A. aeolicus* Hase I is similar to that in standard hydrogenases. However, the reactivation of the former is more than 2 orders of magnitude faster despite the fact that reduction of Ni-B is not thermodynamically more favorable. A scheme for the enzymatic mechanism of *A. aeolicus* Hase I is presented, and the results are discussed in relation to the proposed models of oxygen tolerance.

1. Introduction

Hydrogenases (Hases) are enzymes that catalyze the reversible heterolytic splitting of dihydrogen:[1] $H_2 \rightleftharpoons H^- + H^+ \rightleftharpoons 2H^+ + 2e^-$. They can be classified according to the metal content of their active sites into three distinct classes:[2] [NiFe]-, [FeFe]- and [Fe]- (or iron-sulfur cluster-free) hydrogenases. For all 3 classes, structural information has been derived from X-ray crystallography.[3−7] Most hydrogenases are inhibited by molecular oxygen. This inhibition is reversible for the representatives of the [NiFe] class, whereas for the other two groups exposure to oxygen mostly leads to irreversible degradation. Recently the strict requirement for anaerobic conditions has been re-examined on the grounds of the discovery of enzymes that can perform catalysis under atmospheric conditions. In particular, [NiFe] hydrogenases from hyperthermophilic (e.g., *Aquifex aeolicus*)[8] or Knallgas bacteria (e.g., *Ralstonia eutropha*)[9] have shown increased oxygen tolerance and have allegedly a strong potential to be used in future biotechnological hydrogen-related processes.[10,11] Hereafter, the well-studied oxygen-sensitive [NiFe] enzymes from the *Desulfovibrio* and *Allochromatium* species will be referred to as "standard" hydrogenases to differentiate them from the oxygen tolerant enzymes derived from, for example, *Ralstonia* and *Aquifex* species.

A. aeolicus VF5 is one of the most hyperthermophilic bacteria known to date with an optimum growing temperature of 85 °C.[12] It is a microaerobic, obligate chemolithoautotrophic bacterium

[†] Max-Planck-Institut für Bioanorganische Chemie.
[‡] These authors contributed equally to this work.
[§] Laboratoire de Bioénergétique et Ingénierie des Protéines.

(1) Vignais, P. M. *Results Probl. Cell Differ.* **2008**, *45*, 223–252.
(2) Vignais, P. M.; Billoud, B. *Chem. Rev.* **2007**, *107*, 4206–4272.
(3) Volbeda, A.; Charon, M. H.; Piras, C.; Hatchikian, E. C.; Frey, M.; Fontecilla-Camps, J. C. *Nature* **1995**, *373*, 580–587.
(4) Nicolet, Y.; Lemon, B. J.; Fontecilla-Camps, J. C.; Peters, J. W. *Trends Biochem. Sci.* **2000**, *25*, 138–143.
(5) Shima, S.; Pilak, O.; Vogt, S.; Schick, M.; Stagni, M. S.; Meyer-Klaucke, W.; Warkentin, E.; Thauer, R. K.; Ermler, U. *Science* **2008**, *321*, 572–575.
(6) Armstrong, F. A.; Fontecilla-Camps, J. C. *Science* **2008**, *321*, 498–499.
(7) Ogata, H.; Lubitz, W.; Higuchi, Y. *Dalton Trans.* **2009**, *37*, 7577–7587.
(8) Guiral, M.; Tron, P.; Belle, V.; Aubert, C.; Léger, C.; Guigliarelli, B.; Giudici-Orticoni, M. T. *Int. J. Hydrogen Energy* **2006**, *31*, 1424–1431.
(9) Ludwig, M.; Cracknell, J. A.; Vincent, K. A.; Armstrong, F. A.; Lenz, O. *J. Biol. Chem.* **2009**, *284*, 465–477.
(10) Mertens, R.; Liese, A. *Curr. Opin. Biotechnol.* **2004**, *15*, 343–348.
(11) Lojou, E.; Giudici-Orticoni, M. T.; Bianco, P. *J. Electroanal. Chem.* **2005**, *577*, 79–86.

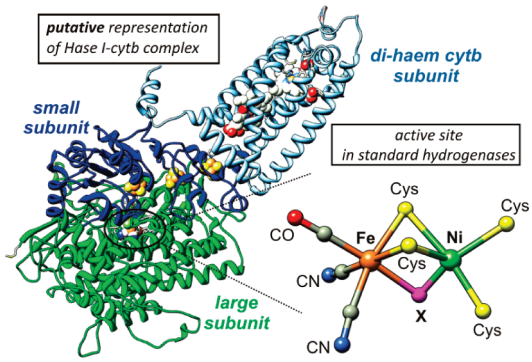

Figure 1. Model of the Hase I-cyt*b* complex from *A. aeolicus* including the small and large subunit of the standard [NiFe] hydrogenase from *D. vulgaris* Miyazaki F (pdb accession code 1WUJ) and the cyt*b* subunit taken from *Wolinella succinogenes* (pdb 2BS2).[16,17] (Right) Structure of the active [NiFe] site including the first coordination ligand sphere.[3,18] The nickel binds 4 cysteine sulfur ligands, two of them bridging to iron, and the iron additionally coordinated by 2 CN^- and 1 CO ligands. X denotes the putative third bridging ligand (see text for details).

that encodes three distinct [NiFe] hydrogenases.[13] Among these enzymes, Hydrogenase I (Hase I) is a membrane attached hydrogenase, which is proposed to be involved in the aerobic respiration using hydrogen as the electron donor. It consists of three subunits (Hase I-cyt*b* complex):[13] a large subunit (70 kDa) that contains the nickel-iron center, a small subunit (40 kDa) that harbors the electron relaying iron-sulfur centers and a dihaem cytochrome *b* subunit (27 kDa), cf. Figure 1. It can also be purified without its native electron acceptor cyt*b*.[13]

Though a crystal structure of the *A. aeolicus* Hase I is not yet available, a combination of techniques has been put forward to characterize its electronic and physicochemical properties. The sequence motif for the binding of the active center in the large subunit is well preserved and electron paramagnetic resonance (EPR) studies have shown nickel signals typical of mesophilic hydrogenases.[13,14] This suggests a similar electronic structure and molecular symmetry of the spin carrying [NiFe] center (Figure 1). Additionally, in the small subunit, the existence of one $[Fe_3S_4]$ and two $[Fe_4S_4]$ clusters has been suggested by the presence of the ten conserved cysteines and one histidine, though the EPR signals were found to be more complex than those in standard hydrogenases (e.g., in *Desulfovibrio*).[13,15]

In oxygen sensitive hydrogenases, the enzyme purified under aerobic conditions is a mixture of two states, namely Ni-A (also called "unready") and Ni-B ("ready"),[19] see Scheme 1. They are both paramagnetic but differ in their spectroscopic and

Scheme 1. Schematic Overview of the Redox Intermediates in Oxygen Sensitive [NiFe] Hydrogenases Obtained from EPR and IR Spectroelectrochemistry[a] [15,19,32]

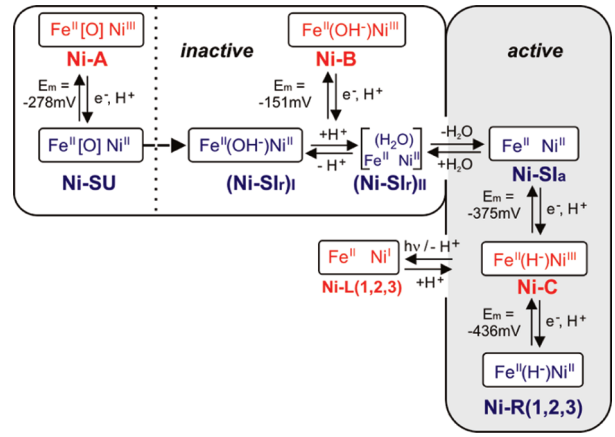

[a] EPR active states are denoted in red and the EPR-silent states in blue. The midpoint potentials for the respective transitions are given for the sulfate reducing bacterium *D. vulgaris* Miyazaki F at pH 7.4,[34] except for the Ni-A/Ni-SU couple which is given at pH 8.2.[35]

catalytic properties.[20,21] Ni-B is readily activated by H_2 or under reducing conditions (hence the name "ready"), whereas Ni-A requires prolonged incubation times. This difference has been attributed to the chemical identity of the oxygenic species present as bridging ligand X in each state (OH^- for Ni-B[22,23] and a putative OOH^- for Ni-A[24,25]). One electron reduction of Ni-A and Ni-B produces the states Ni-SU and Ni-SI_r, respectively[26,27] (Scheme 1), which are EPR-silent (Ni^{2+}). Ni-SI_r exists in two iso-electronic forms; $(Ni\text{-}SI_r)_I$ is in an acid-base equilibrium with a second $(Ni\text{-}SI_r)_{II}$ state, proposed to loosely coordinate a water ligand.[27] After removal of the oxygenic species, the enzyme enters its functional cycle, comprised of three catalytically active states. The most oxidized, Ni-SI_a, is EPR-silent (Ni^{2+}) and its one electron reduction leads to the paramagnetic Ni-C state (Ni^{3+}, $S = {}^1/_2$), with a hydride bridge ($X = H^-$) between the nickel and iron.[28,29] The Ni-C state is light-sensitive at cryogenic temperatures, resulting in the photolytic loss of the hydride ligand with conversion to the Ni-L state(s).[28,30,31] Further reduction of Ni-C yields Ni-R (Ni^{2+}), which is EPR-silent. Up to three different Ni-R states

(12) Huber, R.; Wilharm, T.; Huber, D.; Trincone, A.; Burggraf, S.; Konig, H.; Rachel, R.; Rockinger, I.; Fricke, H.; Stetter, K. O. *Syst. Appl. Microbiol.* **1992**, *15*, 340–351.
(13) Brugna-Guiral, M.; Tron, P.; Nitschke, W.; Stetter, K. O.; Burlat, B.; Guigliarelli, B.; Bruschi, M.; Giudici-Orticoni, M. T. *Extremophiles* **2003**, *7*, 145–157.
(14) Deckert, G.; Warren, P. V.; Gaasterland, T.; Young, W. G.; Lenox, A. L.; Graham, D. E.; Overbeek, R.; Snead, M. A.; Keller, M.; Aujay, M.; Huber, R.; Feldman, R. A.; Short, J. M.; Olsen, G. J.; Swanson, R. V. *Nature* **1998**, *392*, 353–358.
(15) Cammack, R.; Patil, D. S.; Hatchikian, E. C.; Fernandez, V. M. *Biochim. Biophys. Acta* **1987**, *912*, 98–109.
(16) Gross, R.; Simon, J.; Theis, F.; Kröger, A. *Arch. Microbiol.* **1998**, *170*, 50–58.
(17) Gross, R.; Pisa, R.; Sänger, M.; Lancaster, C. R. D.; Simon, J. *J. Biol. Chem.* **2004**, *279*, 274–281.
(18) Higuchi, Y.; Yagi, T.; Yasuoka, N. *Structure* **1997**, *5*, 1671–1680.
(19) Albracht, S. P. J. *Biochim. Biophys. Acta, Bioenerg.* **1994**, *1188*, 167–204.
(20) Fernandez, V. M.; Hatchikian, E. C.; Cammack, R. *Biochim. Biophys. Acta* **1985**, *832*, 69–79.
(21) Lamle, S. E.; Albracht, S. P. J.; Armstrong, F. A. *J. Am. Chem. Soc.* **2004**, *126*, 14899–14909.
(22) van Gastel, M.; Matthias, S.; Brecht, M.; Schroeder, O.; Lendzian, F.; Bittl, R.; Ogata, H.; Higuchi, Y.; Lubitz, W. *J. Biol. Inorg. Chem.* **2006**, *11*, 41–51.
(23) Lubitz, W.; Reijerse, E.; van Gastel, M. *Chem. Rev.* **2007**, *107*, 4331–4365.
(24) Volbeda, A.; Martin, L.; Cavazza, C.; Matho, M.; Faber, B. W.; Roseboom, W.; Albracht, S. P. J.; Garcin, E.; Rousset, M.; Fontecilla-Camps, J. C. *J. Biol. Inorg. Chem.* **2005**, *10*, 239–249.
(25) Ogata, H.; Hirota, S.; Nakahara, A.; Komori, H.; Shibata, N.; Kato, T.; Kano, K.; Higuchi, Y. *Structure* **2005**, *13*, 1635–1642.
(26) De Lacey, A. L.; Hatchikian, E. C.; Volbeda, A.; Frey, M.; Fontecilla-Camps, J. C.; Fernandez, V. M. *J. Am. Chem. Soc.* **1997**, *119*, 7181–7189.
(27) Bleijlevens, B.; van Broekhuizen, F. A.; De Lacey, A. L.; Roseboom, W.; Fernandez, V. M.; Albracht, S. P. J. *J. Biol. Inorg. Chem.* **2004**, *9*, 743–752.
(28) Brecht, M.; van Gastel, M.; Buhrke, T.; Friedrich, B.; Lubitz, W. *J. Am. Chem. Soc.* **2003**, *125*, 13075–13083.
(29) Foerster, S.; van Gastel, M.; Brecht, M.; Lubitz, W. *J. Biol. Inorg. Chem.* **2005**, *10*, 51–62.
(30) Medina, M.; Williams, R.; Cammack, R.; Hatchikian, E. C. *J. Chem. Soc. Faraday Trans.* **1994**, *90*, 2921–2924.

can be observed depending on pH.[27,32] All redox steps are coupled to proton transfer events.[27,32,33] Similar reactions occur upon interaction of the enzyme with molecular hydrogen. The catalytic cycle of these enzymes consists of the states Ni-SI_a, Ni-C and Ni-R. In the case of Hase I from *A. aeolicus*, most of the intermediate states described above for the standard hydrogenases have not yet been identified.

Electrochemical approaches such as protein film electrochemistry[36,37] and electrochemistry in solution[32,38] proved invaluable for the characterization of redox enzymes. In particular, adsorption of hydrogenases on an electrode that substitutes for their physiological redox partner provides a dynamic approach for studying inherent catalytic properties, and delineates reactions both with the substrate and inhibitors.[39−41] Furthermore, *in situ* electrochemistry integrated with Fourier transform infrared (FTIR) spectroscopy has contributed greatly to the characterization of all intermediate states of the standard hydrogenases[32] by relating redox changes in the active site to detectable shifts of the infrared absorption bands, corresponding to the stretching vibrations of the CO, CN^- ligands of the iron.[42,43] This also enables the determination of the number of CN^- and CO ligands at the metals. Some oxygen tolerant enzymes have been proposed to have more than three such ligands bound to the [NiFe] site.[44]

For the *A. aeolicus* Hase I no FTIR data are available and the vibrational frequencies of its redox states are unknown. Although there are some recent, still incomplete studies on oxygen-tolerant enzymes such as *R. eutropha*,[9,45,46] for the *A. aeolicus* Hase I the exact intermediate states, the potentials of the related redox transitions and the activation/inactivation processes have not been elucidated. Thus, in the present study, we combine FTIR spectroscopy to define the structural and redox properties of the intermediates generated in solution, and protein film electrochemistry to characterize the kinetics of (in)activation, either when the enzyme is transiently exposed to O_2 or when its redox state responds to electrode potential steps. The results obtained are compared to those of other hydrogenases (both standard and oxygen tolerant) in order to gain insight into the function of the Hase I from *A. aeolicus* and to better understand the reasons this enzyme is so resistant to oxidative inactivation.

2. Experimental Procedures

2.1. Protein Purification. Isolation and purification of the Hase I from *A. aeolicus* separately or together with its native electron acceptor, a dihaem *b*-type cytochrome, was carried out as previously described[13] in a 50 mM Tris-HCl buffer pH 7.0 in the presence of 5 − 10% glycerol and 0.01% *n*-dodecyl-β-D-maltoside (DDM).

2.2. Electrochemical Measurements-Electrochemistry in-Solution. Electrochemical measurements in solution were carried out in an Optically Transparent Thin Layer Electrochemical (OTTLE) cell designed by Moss et al.[38,47] Twenty-five microliters of 250 μM protein were placed on a 8.5 μm thick gold (Au) minigrid (70% transparent to infrared), which serves as the working electrode. A platinum (Pt) foil is used as the counter and an Ag/AgCl (1 M KCl) as the reference electrode. The cell potential was adjusted by an EG&G 283A potentiostat (Princeton Applied Research). Calibration of the reference electrode prior to and after each measurement was performed by monitoring the reduction of methyl viologen with cyclic voltammetry (−448 mV, pH 7.0). The temperature was regulated in the range 4 to 40 °C by passing water through the metallic body of the cell in a closed external circuit with a thermostat (LAUDA). For the pH dependent redox titrations the buffering solutions used (50 mM concentration) were: MES-NaOH (pH 6.4), HEPES-NaOH (pH 7.4) and Tricine-NaOH (pH 8.4). In the case of the soluble form of Hase I (without cyt*b*) titrations were carried out in the presence of redox mediating agents. The mediators added in the protein solution were: methyl viologen, benzyl viologen, neutral red, phenosafranine, anthraquinone-2-sulfonate, anthraquinone-1,5-disulfonate, 2-hydroxy-1,4-naphthoquinone, potassium indigo tetrasulfonate, methylene blue, phenazine methosulfate and naphthoquinone. Their redox potentials and pH dependence have been reported elsewhere.[48,49] Their relative concentration with respect to the protein content was 1:3. Potentiometric titrations of the Hase I copurified with the cyt*b* were carried out in the absence of any electron-transfer reagents to avoid inhibition of the quinone binding site of cyt*b*. In all solutions, KCl was added to a final concentration of 150 mM. Results with or without electron mediating agents in solution are similar, although longer equilibration times are required in the absence of mediators. After each potential step, an equilibration time of 10-15 min was allowed prior to recording the infrared spectra in the absence of mediators, while in the presence of mediators the equilibration time was shortened to 3 min. All potentials referred in the present work are quoted with respect to the standard hydrogen electrode potential (SHE).

2.3. Electrochemical Measurements-Protein Film Electrochemistry (PFE). In protein film electrochemistry, electron transfer between the electrode and the enzyme is direct, and the activity is measured as a current (positive = oxidation, negative = reduction) whose magnitude is proportional to the turnover rate.[36,37,50] The fact that the active site of the enzyme is buried in the protein does not preclude a fast electron transfer, provided it is "wired" to the electrode by a chain of redox centers that permits fast intramolecular electron exchange.[51] In *A. aeolicus* Hase I, like in the prototypical

(31) Kellers, P.; Pandelia, M. E.; Currell, L. J.; Görner, H.; Lubitz, W. *Phys. Chem. Chem. Phys.* **2009**, *11*, 8680–8683.
(32) De Lacey, A. L.; Fernandez, V. M.; Rousset, M.; Cammack, R. *Chem. Rev.* **2007**, *107*, 4304–4330.
(33) Léger, C.; Jones, A. K.; Roseboom, W.; Albracht, S. P. J.; Armstrong, F. A. *Biochemistry* **2002**, *41*, 15736–15746.
(34) Fichtner, C.; Laurich, C.; Bothe, E.; Lubitz, W. *Biochemistry* **2006**, *45*, 9706–9716.
(35) Millo, D.; Pandelia, M. E.; Utesch, T.; Wisitruangsakul, N.; Mroginski, M. A.; Lubitz, W.; Hildebrandt, P.; Zebger, I. *J. Phys. Chem. B* **2009**, *113*, 15344–15351.
(36) Vincent, K. A.; Parkin, A.; Armstrong, F. A. *Chem. Rev.* **2007**, *107*, 4366–4413.
(37) Léger, C.; Bertrand, P. *Chem. Rev.* **2008**, *108*, 2379–2438.
(38) Best, S. P. *Coord. Chem. Rev.* **2005**, *249*, 1536–1554.
(39) Léger, C.; Dementin, S.; Bertrand, P.; Rousset, M.; Guigliarelli, B. *J. Am. Chem. Soc.* **2004**, *126*, 12162–12172.
(40) Jones, A. K.; Lamle, S. E.; Pershad, H. R.; Vincent, K. A.; Albracht, S. P. J.; Armstrong, F. A. *J. Am. Chem. Soc.* **2003**, *12*, 8505–8514.
(41) Vincent, K. A.; Parkin, A.; Lenz, O.; Albracht, S. P. J.; Fontecilla-Camps, J. C.; Cammack, R.; Friedrich, B.; Armstrong, F. A. *J. Am. Chem. Soc.* **2005**, *127*, 18179–18189.
(42) Happe, R. P.; Roseboom, W.; Pierik, A. J.; Albracht, S. P. J.; Bagley, K. A. *Nature* **1997**, *385*, 126.
(43) Pierik, A. J.; Roseboom, W.; Happe, R. P.; Bagley, K. A.; Albracht, S. P. J. *J. Biol. Chem.* **1999**, *274*, 3331–3337.
(44) Happe, R. P.; Roseboom, W.; Egert, G.; Friedrich, C. G.; Massanz, C.; Friedrich, B.; Albracht, S. P. J. *FEBS Lett.* **2000**, *466*, 259–263.
(45) Saggu, M.; Zebger, I.; Ludwig, M.; Lenz, O.; Friedrich, B.; Hildebrandt, P.; Lendzian, F. *J. Biol. Chem.* **2009**, *284*, 16264–16276.
(46) Burgdorf, T.; Löscher, S.; Liebisch, P.; van der Linden, E.; Galander, M.; Lendzian, F.; Meyer-Klaucke, W.; Albracht, S. P. J.; Friedrich, B.; Dau, H.; Haumann, M. *J. Am. Chem. Soc.* **2005**, *127*, 576–592.
(47) Moss, D. A.; Leonhard, M.; Bauscher, M.; Mäntele, W. *FEBS Lett.* **1991**, *283*, 33–36.
(48) Fultz, M. L.; Durst, R. A. *Anal. Chim. Acta* **1982**, *140*, 1–18.
(49) Prince, R. C.; Linkletter, S. J. G.; Dutton, P. L. *Biochim. Biophys. Acta* **1981**, *635*, 132–148.
(50) Armstrong, F. A.; Belsey, N. A.; Cracknell, J. A.; Goldet, G.; Parkin, A.; Reisner, E.; Vincent, K. A.; Wait, A. F. *Chem. Soc. Rev.* **2009**, *38*, 36–51.
(51) Léger, C.; Lederer, F.; Guigliarelli, B.; Bertrand, P. *J. Am. Chem. Soc.* **2006**, *128*, 180–187.

[NiFe] enzymes from *A. vinosum* and *D. fructosovorans*, this chain consists of iron-sulfur clusters ([FeS][3,52]), one of which is exposed at the surface of the enzyme and can directly exchange electrons either with the electrode or the soluble redox partner. The exact amount of enzyme adsorbed onto the electrode is unknown, and therefore the absolute value of the turnover rate cannot be deduced. However, provided that the electroactive coverage is constant, any relative change in the current can be interpreted to result from a change in activity. In many cases film desorption also contributes to the decrease in current over time.[53] *A. aeolicus* Hase I, however, forms very stable films when adsorbed onto a rotating pyrolytic graphite edge electrode (the typical time constant of the decay is about one to two hours if the temperature remains below 45 °C). This makes data interpretation straightforward, as shown in the main text.

Protein film electrochemistry experiments (cyclic voltammetry and chronoamperometry) were carried out in a glovebox filled with N_2, using the electrochemical setup and equipment previously described.[39] The two-compartment electrochemical cell was thermostatted at the desired temperature value using a water circulation system. The rotating pyrolytic graphite edge working electrode (PGE) (area A $\approx$ 3 mm^2) was used in conjunction with an electrode rotator, a platinum wire was used as a counter electrode, and a saturated calomel electrode (SCE), located in a side arm containing 0.1 M NaCl and maintained at room temperature, was used as a reference. All potentials are quoted versus the standard hydrogen electrode (SHE), $E_{SHE} = E_{SCE} + 241$ mV.

The electrochemical cell contained a buffer mixture of MES, CHES, TAPS, HEPES and sodium acetate (5 mM each) and 0.1 M NaCl; the temperature (*T*) and pH are indicated in each caption. Hase I was adsorbed onto the pyrolytic graphite electrode as previously described;[39] protein films were prepared by painting the electrode with about half a microliter of a stock enzyme solution (~5−10 μM of enzyme in the mixed buffer at pH 7). The enzyme-coated electrode was inserted in the electrochemical cell containing the buffer mixture at pH 7, 40 °C, under an atmosphere of H_2. The low potential poise that we use to activate standard hydrogenases[39] made no difference in the intensity of the signal, consistent with the earlier observation that the enzyme shows no lag in solution assays of H_2 oxidation.[8]

For determining the kinetics of O_2 inhibition, we employed methods we have previously developed to characterize oxygen sensitive enzymes.[39,54−56] The activity is measured at a fixed potential, after small aliquots of a buffer, saturated with pure oxygen at room temperature and kept in a capped serum bottle, are injected with gastight syringes into the cell solution, which is continuously flushed with H_2. For the experiments in Figure 7, where O_2 is added in the cell while the enzyme is oxidizing H_2 under one atmosphere of H_2, we injected a volume of 200 μL into a 3 mL buffer; this leads to an instant decrease in H_2 concentration of about 6%. As the K_m of the enzyme for H_2 is small, the dilution of H_2 upon injecting the oxygen-saturated solution does not significantly decrease the turnover rate. This is demonstrated in Figure S1 of the Supporting Information, which shows that when 500 μL of solution saturated with N_2 is injected in a 3 mL solution saturated with H_2, the H_2-oxidation catalytic current decreases by only 1.5%. The bimolecular rates of inhibition are converted to units of $s^{-1}(atm(air))^{-1}$ considering that atmospheric air contains 21% O_2. The concentrations of O_2 were calculated using the Henry constants 1.25 $mM(atm(O_2))^{-1}$.

The electrochemical data were analyzed with a program called SOAS,[57] which is available for download from the web: http://bip.cnrs-mrs.fr/bip06/.

2.4. Fourier Transform Infrared (FTIR) Spectroscopy. Infrared measurements were carried out on a Bruker IFS 66v/s FTIR spectrometer with 2 cm^{-1} resolution. The detector was a photovoltaic mercury-cadmium-telluride (MCT) element (Kolmar Technologies). The sample chamber was purged with N_2 to avoid contributions in the spectra from vapor absorption. The software for data recording consisted of the OPUS package (Bruker Optics). Analysis and further processing was performed with MATLAB 6.5 (Mathworks). For the potentiometric titrations the CO peak absorption intensities at each potential value corresponding to all the redox states were added. The individual peak intensities of the respective states were further normalized by dividing by the sum of all peak intensities for that potential value. The sum of all the individual normalized intensities equals to unity. For the titrations these normalized IR intensities of each redox intermediate have been plotted as a function of the applied potential (vs SHE); see Supporting Information for a detailed description. For the experiments at temperatures below 200 K, an Oxford Instruments OptistatCF cryostat with an ITC 503 temperature controller was used. Illumination of the samples in the cryostat was performed by a slide projector (halogen lamp, 24 V, 250 W).

2.5. EPR Spectroscopy. EPR measurements were carried out with a continuous wave (cw) E-300 X-band spectrometer (at ~9.4 GHz) equipped with a rectangular cavity (TE_{102}) and an Oxford Instruments helium flow cryostat with an ITC 503 temperature controller.

3. Results

The [NiFe] hydrogenase from the hyperthermophilic bacterium *A. aeolicus* has been obtained in two forms; as a heterodimeric enzyme consisting of the [NiFe] site and the iron-sulfur clusters (Hase I) and as a heterotrimer including additionally the dihaem *b*-type cytochrome subunit (Hase I-cyt*b*). The protein film electrochemistry experiments were performed on the soluble Hase I, while the solution redox titrations were carried out for both forms at 4, 25, and 40 °C. The spectroelectrochemical results were identical within error for all temperatures, thus only the data at 25 °C are shown. Potentiometric titrations of the Hase I-cyt*b* complex were carried out in the absence of any electron-transfer mediators to avoid interaction with the quinone binding site of cyt*b*. All processes were reversible and independent of the addition of mediators.

3.1. FTIR-Electrochemistry in Solution. Infrared spectroscopy detects the absorbance corresponding to the vibrations of the diatomic ligands bound to the active site, which appear in the spectra as bands at specific frequency positions. For the intrinsic ligands to Fe, bands in the region from 1970 to 1900 cm^{-1} are associated with the CO stretching vibrations, while bands between 2105 and 2040 cm^{-1} are related to the coupled CN^- vibrations. These values are similar in enzymes derived from different species.[32] Transitions between the possible redox intermediates are observed as shifts of these bands toward lower

(52) Dementin, S.; Belle, V.; Bertrand, P.; Guigliarelli, B.; Adryanczyk-Perrier, G.; De Lacey, A. L.; Fernandez, V. M.; Rousset, M.; Léger, C. *J. Am. Chem. Soc.* **2006**, *128*, 5209–5218.
(53) Fourmond, V.; Lautier, T.; Baffert, C.; Leroux, F.; Liebgott, P. P.; Dementin, S.; Rousset, M.; Arnoux, P.; Pignol, D.; Meynial-Salles, I.; Soucaille, P.; Bertrand, P.; Léger, C. *Anal. Chem.* **2009**, *81*, 2962–2968.
(54) Baffert, C.; Demuez, M.; Cournac, L.; Burlat, B.; Guigliarelli, B.; Bertrand, P.; Girbal, L.; Léger, C. *Angew. Chem., Int. Ed.* **2008**, *47*, 2052–2054.
(55) Liebgott, P. P.; Leroux, F.; Burlat, B.; Dementin, S.; Baffert, C.; Lautier, T.; Fourmond, V.; Ceccaldi, P.; Cavazza, C.; Meynial-Salles, I.; Soucaille, P.; Fontecilla-Camps, J. C.; Guigliarelli, B.; Bertrand, P.; Rousset, M.; Léger, C. *Nat. Chem. Biol.* **2009**, *6*, 63–70.
(56) Leroux, F.; Dementin, S.; Burlat, B.; Cournac, L.; Volbeda, A.; Champ, S.; Martin, L.; Guigliarelli, B.; Bertrand, P.; Fontecilla-Camps, J. C.; Rousset, M.; Léger, C. *Proc. Nat. Acad. Sci. U.S.A.* **2008**, *105*, 11188–11193.
(57) Fourmond, V.; Hoke, K.; Heering, H. A.; Baffert, C.; Leroux, F.; Bertrand, P.; Léger, C. *Bioelectrochem.* **2009**, *76*, 141–147.

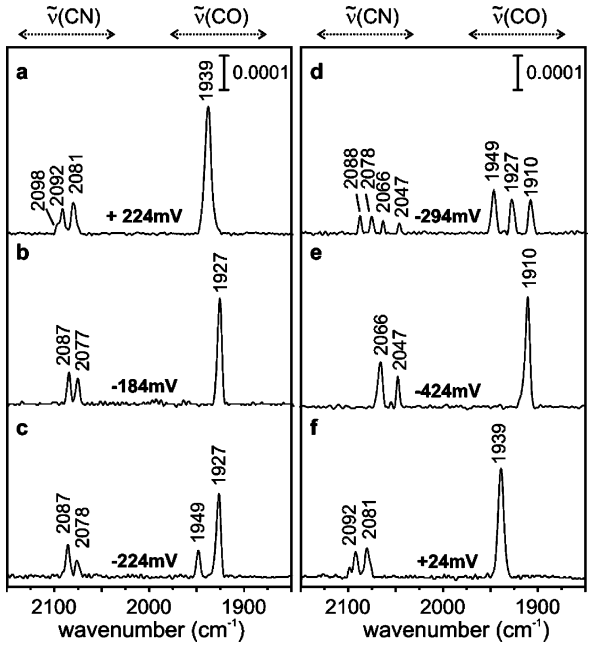

Figure 2. FTIR spectra of the Hase I-cyt*b* complex from *A. aeolicus* at 25 °C, pH 7.4. (a) the as-isolated enzyme at the resting potential of +224 mV, (b) enzyme after full activation poised at −184 mV, (c) at −224 mV, (d) at −294 mV, (e) at −424 mV and (f) reoxidized at +24 mV. The protein solution did not contain any electron mediating reagents.

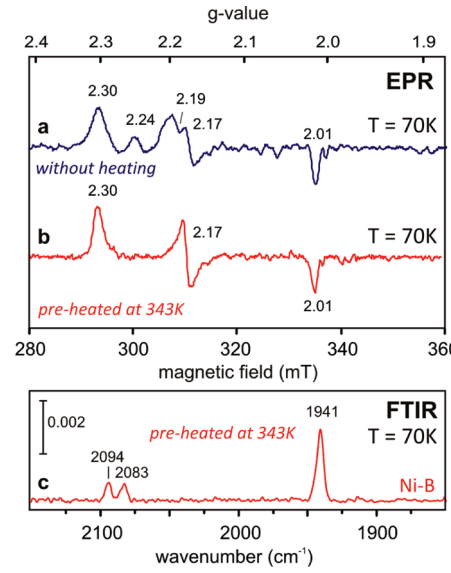

Figure 3. (a) EPR spectrum of the "as-isolated" Hase I from *A. aeolicus*, (b) EPR spectrum of the as-isolated Hase I after heating the enzyme at 343 K (70 °C) for 15 min and then freezing it in a cold ethanol/liquid N_2 bath. Both spectra were recorded at 70 K. (c) Low-temperature FTIR spectrum (at 70 K) of the "preheated" enzyme. Other experimental conditions: (EPR) microwave frequency 9.456 GHz, microwave power 10 mW, modulation amplitude 1 mT, (FTIR): resolution 2 cm^{-1}, 2000 averages.

or higher frequencies, and are correlated with an increase or a decrease in the electron density at the Fe, respectively.[58] Such shifts result from changes in the coordination number of the Fe ion, in the hydrogen bonding of the CN^- ligands with nearby amino-acids, in the electronic state of the nickel and more generally in the electron delocalization at the [NiFe] site.[59−61] Therefore, this set of three bands is characteristic for the electronic and structural details of the active site and can accurately describe each redox state.

3.1.1. Oxidized Inactive Enzyme.

Ni-B. Figure 2a shows the FTIR spectrum of the as isolated Hase I-cyt*b* complex from *A. aeolicus* at a resting potential of +224 mV at 25 °C and pH 7.4 in the absence of any redox mediators. In this spectrum three main bands are observed; one CO stretching vibration at 1939 cm^{-1} and two CN^- vibrations at 2081 and 2092 cm^{-1}. This shows that the coordination of the active site with respect to standard hydrogenases is found to be preserved and consistent with a $Fe(CN)_2CO$ moiety. On the basis of the EPR spectrum of the as-purified enzyme[13] (also cf Figure 3) and of previous studies on hydrogenases, this set of peaks corresponds to the Ni-B state[23,32] (see Table 1 and Supporting Information). The related FTIR bands for an oxygen-sensitive (*D. fructosovorans*)[62] and an oxygen-tolerant (MBH *R. eutropha*)[45] hydrogenase are included for comparison. A band of low intensity at 2098 cm^{-1} and a shoulder at 2079 cm^{-1} are also observed, but this is neither related to Ni-A nor to extra CN^- ligands as will be discussed in the following. The absence of Ni-A and the presence only of Ni-B in the FTIR (and EPR)[13] is consistent with the observation (described below) that the enzyme is quickly activated and indicates an electronic configuration of the active center in this state that is similar to the oxygen-sensitive hydrogenases.

3.1.2. Enzyme Activation in the Electrochemical Cell. Ni-SI_a. The enzyme could be fully activated in the electrochemical cell at 25 °C by applying a potential of −326 mV for 20 min. The protein was subsequently reoxidized at +100 mV. The obtained spectrum is identical to that of Figure 2a, which excludes that the low intensity band at 2098 cm^{-1} corresponds to any of the unready states (i.e., Ni-A, Ni-SU), since reoxidation in the electrochemical cell (anaerobic) leads only to the "ready" inactive state Ni-B.[27,32] At a potential of −184 mV all the bands shift toward lower frequencies (Figure 2b). The CO band appears at 1927 cm^{-1} and the two coupled CN^- shift to 2077 and 2087 cm^{-1}, respectively. Such shifts are consistent with a reduction of the Ni-B state to an EPR-silent (Ni^{2+}, d^8) species. According to the mechanistic scheme of the standard hydrogenases, this state should correspond to $(Ni\text{-}SI_r)_I$. However, by taking into account that the CN^- stretching vibrations of a specific redox state are within 0-6 cm^{-1} similar to [NiFe] enzymes from different organisms, the CN^- bands in Figure 2b resemble more closely those of the Ni-SI_a[63,64] state and not those of $(Ni\text{-}SI_r)_I$ (see Table 1, Table S1, Supporting Information). This indicates that the latter does not accumulate sufficiently to be detected.

(58) Bagley, K. A.; Duin, E. C.; Roseboom, W.; Albracht, S. P. J.; Woodruff, W. H. *Biochemistry* **1995**, *34*, 5527–5535.
(59) Lai, C. H.; Lee, W. Z.; Miller, M. L.; Reibenspies, J. H.; Darensbourg, D. J.; Darensbourg, M. Y. *J. Am. Chem. Soc.* **1998**, *120*, 10103–10114.
(60) De Lacey, A. L.; Santamaria, E.; Hatchikian, E. C.; Fernandez, V. M. *Biochim. Biophys. Acta, Protein Struct. Mol. Enzymol.* **2000**, *1481*, 371–380.
(61) Darensbourg, M. Y.; Lyon, E. J.; Smee, J. J. *Coord. Chem. Rev.* **2000**, *206*, 533–561.
(62) De Lacey, A. L.; Stadler, C.; Fernandez, V. M.; Hatchikian, E. C.; Fan, H. J.; Li, S. H.; Hall, M. B. *J. Biol. Inorg. Chem.* **2002**, *7*, 318–326.
(63) The stretching vibrations corresponding to the Ni-SI_a and the $(Ni\text{-}SI_r)_{II}$ are reported to be identical within error.[27] Thus, the loosely bound water ligand in $(Ni\text{-}SI_r)_{II}$ is suggested to affect the electronic density only slightly leading to shifts that are difficult to resolve in the FTIR spectra. At temperatures ≥25°C the loosely bound water ligand is easily liberated leading to Ni-SI_a within a fraction of a second, which is the case in our experiments (25, 40 °C).
(64) Kurkin, S.; George, S. J.; Thorneley, R. N. F.; Albracht, S. P. J. *Biochemistry* **2004**, *43*, 6820–6831.

Table 1. Comparison of the Infrared Stretching Vibrations of the CO and CN^- Diatomic Ligands of the [NiFe] Hydrogenases from *A. aeolicus*, *D. fructosovorans* and *R. eutropha* (MBH) at 25 °C[a]

	A. aeolicus[b]			*D. fructosovorans*[c]			*R. eutropha* (MBH)[d]		
state	$\bar{\nu}_{CO}$ (cm^{-1})	$\bar{\nu}_{CN^-asym}$ (cm^{-1})	$\bar{\nu}_{CN^-sym}$ (cm^{-1})	$\bar{\nu}_{CO}$ (cm^{-1})	$\bar{\nu}_{CN^-asym}$ (cm^{-1})	$\bar{\nu}_{CN^-sym}$ (cm^{-1})	$\bar{\nu}_{CO}$ (cm^{-1})	$\bar{\nu}_{CN^-asym}$ (cm^{-1})	$\bar{\nu}_{CN^-sym}$ (cm^{-1})
Ni-B	1939	2081	2092	1946	2080	2091	1948	2081	2098
Ni-SI_a	1927	2077	2087	1933	2074	2087	1936	2075	2093
Ni-C	1949	2078	2088	1951	2074	2086	1957	2075	2097
Ni-R2	1910	2047	2066	1922	2051	2067	1921	2048	2064
Ni-X[e]	–	2079	2098	nd	nd	nd	1943	2082	2104

[a] Error in the values is ±1 cm^{-1}. [b] Data from this work. [c] Data from ref 62. [d] Data from ref 45; nd stands for not determined. [e] Values assigned to the unknown state Ni-X that is putatively assigned to a readily activated state, which is EPR-active (see text, Figure 3 and Supporting Information).

When the experiment was performed at 4 °C to decelerate the inactivation,[27] no additional bands could be observed that could be associated with $(Ni\text{-}SI_r)_I$. At this temperature, the bands of the EPR-silent state assigned to the Ni-SI_a, shifted by approximately 1-2 wavenumbers. This small shift was reversible at higher temperatures and it might correspond to the formation of the "inactive"$(Ni\text{-}SI_r)_{II}$, likely to occur under these conditions (4 °C). These shifts were more pronounced in samples reduced with H_2 and left at 4°C in the IR cell for several hours (> 4h) (Figure S2, Supporting Information).

Ni-C. Lowering the potential further to −224 mV led to the appearance of a redox intermediate with a CO vibration at 1949 cm^{-1} and CN^- bands very similar to those of the Ni-SIa state (Figure 2c, Table 1). This spectrum is consistent with the appearance of the catalytically active Ni-C state, which carries a hydride ligand (H^-)[28] that can be photodissociated at temperatures lower than 170 K[31,58] (Scheme 1). To confirm this, the Hase I-cyt*b* complex was reduced with H_2 and the sample was subsequently examined using EPR and FTIR at cryogenic temperatures (100 K). A rhombic signal with g-values 2.21, 2.15, and 2.01 confirmed the presence of Ni-C, which upon illumination converted to a light-induced form with g-values 2.28, 2.12, and 2.05 (Ni-L2 state). Illumination of the sample in the FTIR at the same temperature resulted in the disappearance of only the 1949 cm^{-1} CO band and its related CN^- bands, demonstrating that these can be uniquely assigned to the Ni-C state. In the FTIR titration, the amount of Ni-C is almost maximal at a potential of −294 mV and corresponded to 35-40% of the enzyme molecules (Figure 2d), as estimated from the integrated intensity of the CO band corresponding to this state.

Ni-R. Ni-C is formed in substoichiometric amounts and converts at slightly more negative potentials to another state, characterized by one CO band at 1910 cm^{-1} and two CN^- stretching bands at 2047 and 2066 cm^{-1} (−424 mV, Figure 2e). This appears to be the most reduced state of the enzyme, as no further spectral changes take place by applying more negative potentials. This intermediate is thus assigned to the Ni-R state (EPR-silent, Ni^{2+}). On the basis of the stretching vibrations, the observed Ni-R in Hase I is not the typical form (Ni-R1) found in mesophilic hydrogenases[32,45] at neutral pH (both anaerobic and aerobic), but resembles more the so-called Ni-R2 state (Table S2, Supporting Information).

3.1.3. Reoxidation in the Electrochemical Cell. Reoxidation of the enzyme at +24 mV resulted in the infrared spectrum shown in Figure 2f, which again corresponds to the Ni-B state (Table 1). The CN^- band at 2098 cm^{-1} is also present, showing that it is related neither to the Ni-A nor to the Ni-SU states. Interestingly, at the same position relative to the high-frequency CN^- peak belonging to Ni-B, an additional band of similar small intensity has also been observed in the case of the as-isolated/reoxidized membrane bound hydrogenase (MBH) from *R. eutropha*.[45] In the case of *A. aeolicus* the second CN^- band vibrationally coupled to the 2098 cm^{-1} band is most likely observed as a shoulder of the 2081 cm^{-1} peak at 2079 cm^{-1}. The corresponding CO band is not resolved, presumably due to an overlap with that of the Ni-B state. These additional FTIR spectroscopic features (Figures 2a, f) can therefore correspond to a slightly different conformation of another readily activated oxidized state (Ni-X).

Electron paramagnetic resonance experiments have shown that at such positive potentials an additional state is present (Figure 3, Figure S3, Supporting Information). This state is different from Ni-A and could be identified by pulsed Q-band EPR spectroscopy because it has different relaxation properties compared to Ni-B and the iron-sulfur clusters (Figure S4, Supporting Information). Further experiments were performed on frozen solutions of as-isolated enzyme preparations that were incubated, prior to the measurements, for 15 min at 70 °C (close to the enzyme's physiological temperature). The resulting findings are shown in Figure 3, in which the extra signals are now absent from both the EPR and FTIR spectra. The additional features in the infrared measurements can be thus related to the paramagnetic state denoted Ni-X. The yield of the latter is substoichiometric relative to Ni-B and varies between different samples (e.g., 16−30% of the paramagnetic states with the rest of the molecules being in the Ni-B state). Further experiments are needed to obtain a more detailed picture of the active site conformation in this state.

3.1.4. Potentiometric Titration at pH 7.4 (Hase I-cyt*b*). Figure 4A shows the potentiometric titration for the Hase I-cyt*b* complex at pH 7.4, in which the redox transitions between different states are monitored via changes in the infrared spectra as a function of the applied potential. FTIR spectra were recorded with potential steps of 20 mV. The normalized absorption of all states was fitted as described in the Supporting Information by assuming all transitions correspond to one-electron processes. Activation of the enzyme starting from the Ni-B state resulted in Ni-SI_a, without the $(Ni\text{-}SI_r)_I$ state being a detectable intermediate. This redox transition corresponds to a one-electron process with an apparent midpoint potential of −105 mV. The Ni-SI_a/Ni-C couple has a value of −295 mV, while the midpoint potential for the Ni-C/Ni-R couple was estimated to be −300 mV. All processes were fully reversible and the error in the value determination is ±10 mV.

3.1.5. Potentiometric Titration at pH 7.4 (Hase I). The potentiometric titration corresponding to the Hase I without the cyt*b* at pH 7.4 is presented in Figure 4B. Results were within error identical to those obtained for the Hase I-cyt*b* enzyme (Table 2). The only difference is related to the Ni-C intermediate. Ni-C appears in the same potential range as in the case of Hase I-cyt*b*; however it is of a significant lower yield. Such difference may result from the presence of mediators that were used for titrating

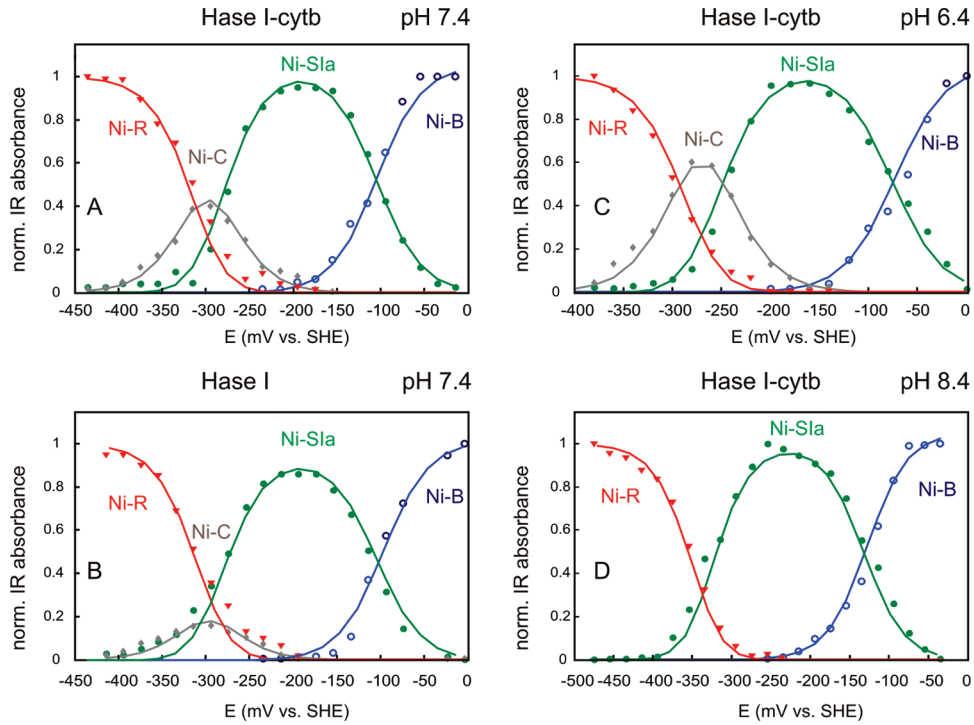

Figure 4. Potential dependent behavior of the redox intermediates of the Hase I from *A. aeolicus* at three different pH values, (A) 7.4 (with cyt*b*), (B) 7.4 (without cyt*b*), (C) 6.4 (with cyt*b*), and (D) 8.4 (with cyt*b*). The temperature was 25 °C and redox mediators were present in solution only for the case of Hase I without the cyt*b*. Note that the direction of the *x* axis from right to left goes from high to low potentials. Different *x* scales are used for different pH values.

Table 2. Midpoint Redox Potentials for the Intermediate Redox States of the Hase I-cyt*b* from *A. aeolicus* at Different pH Values and Comparison with Those Measured for Hase I at pH 7.4[a]

pH	Ni-B/Ni-SIa couple	Ni-SIa/Ni-C couple	Ni-C/Ni-R couple
		Hase I-cyt*b*	
6.4	−73	−264	−270
7.4	−105	−295	−300
8.4	−128	−340	−340
		Hase I	
7.4	−105	−295	−297

[a] Potentials are quoted vs the standard hydrogen electrode potential (SHE). The error is ±10 mV.

the Hase I alone (without the cytochrome *b*); it may also occur that the presence of the cytochrome slightly stabilizes the Ni-C state, although the mechanism by which the active site could sense the remote subunit remains to be determined.

3.1.6. Effect of pH on the Redox Processes. The potentiometric titrations of the Hase I-cyt*b* complex were carried out also for pH values 6.4 and 8.4, see Figures 4C and D, respectively. At pH 6.4 the yield of the Ni-C state was increased, in agreement with previous observations on standard hydrogenases.[26,27] However, at a higher pH of 8.4, the Ni-C could not be detected as an intermediate in the reduction from Ni-SI_a to Ni-R, which shows that in a more basic environment this state becomes less stable. The reduction potentials for all intermediates were pH-dependent demonstrating that the redox processes are coupled to proton transfer (Table 2).

An additional result of these titrations was that only one Ni-R state can be observed. This finding was unexpected, since Ni-R commonly exists in more than one protonation state(s), depending on pH.[32] Such a situation does not apply for Ni-R in Hase I-cyt*b*. At all three pH values examined, no additional bands associated with different forms of this most reduced state of the enzyme were detected (Figure S5 in Supporting Information). Furthermore, the change in pH did not result in the appearance of additional signals that could be related to the (Ni-SI_r)$_I$ state, as has been observed previously in standard hydrogenases. This is likely to result from differences in inherent thermodynamic properties that govern the reactivation of the complex, such as the pK_a of the amino acid participating in the transition from (Ni-SI_r)$_I$ to (Ni-SI_r)$_{II}$/Ni-SI_a in standard hydrogenases.

The above IR electrochemical experiments yielded information on the detectable redox intermediates of Hase I, their spectroscopic IR signatures as well as the midpoint potentials of the transitions involved. In the next section, our study is extended by using protein film electrochemistry (PFE) with the aim to determine the catalytic properties of Hase I and to study the reaction of the enzyme with O_2.

3.2. Protein Film Electrochemistry. 3.2.1. Catalytic Activity of Hase I. Figure 5 shows a typical voltammetric signature of *A. aeolicus* Hase I, from which several important properties of the enzyme can be derived[73] and compared to those of other [NiFe] hydrogenases.[41,65,66]

Under oxidative conditions the enzyme reversibly inactivates; as the potential is scanned above 0 mV vs SHE the H_2-oxidation current decreases, while activity is recovered on the reverse scan. This anaerobic oxidative inactivation has been observed with all [NiFe] hydrogenases characterized to date; it corresponds to the reversible formation of the "ready" inactive state Ni-B.[36]

(65) Cracknell, J. A.; Wait, A. F.; Lenz, O.; Friedrich, B.; Armstrong, F. A. *Proc. Nat. Acad. Sci. U.S.A.* **2009**, *106*, 20681–20686.
(66) Lukey, M. J.; Parkin, A.; Roessler, M. M.; Murphy, B. J.; Harmer, J.; Palmer, T.; Sargent, F.; Armstrong, F. A. *J. Biol. Chem.* **2010**, *285*, 3928–3938.

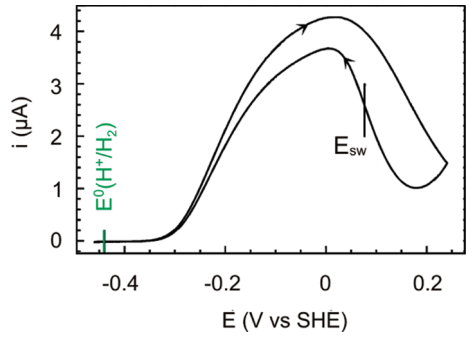

Figure 5. Cyclic voltammogram showing the anaerobic oxidative inactivation and reductive activation of *A. aeolicus* Hase I adsorbed on a rotating disk graphite electrode. Arrows mark the direction of the scan. The hydrogen oxidation activity decreases above $E = 20$ mV, when the potential is being swept upward, and it is recovered on the reverse scan. The reduction potential of the hydrogen couple $E^0(H^+/H_2)$ is marked by a green vertical line. The parameter E_{sw} (switch potential) denotes the position of the first inflection point of the scan toward low potentials. Experimental conditions: pH 7, $T = 40$ °C, 1 bar H_2. The enzyme-coated electrode was rotated at a high rate ($\omega = 4$ krpm) to avoid any limitation from mass transport of H_2, and the electrode potential was swept slowly ($\upsilon = 0.3$ mV/s).

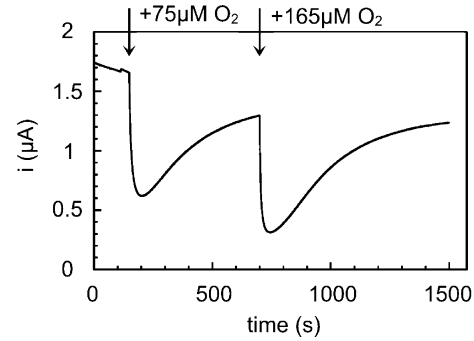

Figure 6. Change in hydrogen oxidation activity (current i) of *the A. aeolicus* Hase I, measured at $E = +210$ mV after addition of two oxygen-saturated buffer aliquots into the electrochemical cell solution. The final concentrations were 75 and 165 μM, respectively, before O_2 was flushed away from the solution by a stream of hydrogen. The potential was stepped from the open-circuit potential (OCP) to +210 mV and held for 650 s prior to recording the signal shown here, during which the activity decreases by about 70% (consistent with the observations in Figure 7, see below). Experimental conditions: pH 7, $T = 40$ °C, 1 bar H_2.

No reductive activity is observed at low potentials, demonstrating that the Hase I from *A. aeolicus* is a much more efficient catalyst for H_2 oxidation than H_2 production. This agrees with the previous observation that Hase I can reduce protons at low potentials and under N_2 atmosphere,[67] but only with a maximal rate that is much lower than the maximal rate of H_2 oxidation. In this respect, *A. aeolicus* Hase I resembles the membrane bound enzyme (MBH) from *R. eutropha* (Figure 2 in ref 68) and differs from the prototypical *D. fructosovorans* enzyme, which shows significant H^+ reduction activity (Figure 1 in ref 39).

The vertical line at +77 mV in Figure 5 marks the value of the so-called "switch potential", E_{sw}, which represents the point on the scan toward low potentials where the activity switches back on. This parameter is a phenomenological marker of oxygen tolerance, since the greater E_{sw}, the easier the reductive activation of the enzyme. Indeed, the values of E_{sw} in the case of the *A. aeolicus*, *R. eutropha*[68] and *E. coli* Hyd-1[66] enzymes are about 200 mV more positive than in oxygen-sensitive hydrogenases.[40] For the *A. vinosum* hydrogenase, there is a fair agreement between the value of E_{sw} and the reduction potential of the Ni-B species.[40] This, however, is not the case for *A. aeolicus* Hase I: E_{sw} (Figure 5) is about 180 mV above the reduction potential of Ni-B (Table 2).

Figure 6 shows the result of a chronoamperometric experiment aimed at studying the inhibition by O_2. This consists of injecting into the electrochemical cell aliquots of solutions saturated with O_2 while the enzyme is oxidizing H_2. The resulting dilution of H_2 is negligible (cf Methods and Figure S1, Supporting Information). The electrode potential is high in this experiment, to avoid reduction of O_2 on the electrode.[39] We added successively in the electrochemical cell two aliquots of O_2 saturated buffer to achieve final concentrations of 75 and 165 μM, respectively. After each injection, the oxygen concentration initially increases (the mixing time is lower than 0.1s) and then exponentially decreases with a typical time constant of about 15s (the exact value depended on the experimental conditions, and was measured independently by monitoring direct O_2 reduction on a bare electrode poised at a low potentials, as described in ref 39). Figure 6 shows that after oxygen is injected, the catalytic current resulting from hydrogen oxidation activity quickly drops, but it is fully recovered after oxygen has been flushed away. This agrees with a previous study, where *A. aeolicus* Hase I was shown to retain an H_2 oxidizing ability even after exposure to approximately 100 μM O_2 at 60 °C.[67]

The results presented in Figure 6 for *A. aeolicus* are similar to those reported for the oxygen-tolerant MBH enzyme from *R. eutropha*.[69] In contrast, standard hydrogenases are irreversibly inactivated by O_2 under such oxidizing conditions, and their activity is recovered only after reduction.[21,39]

3.2.2. Kinetics of (In)Activation; Reaction with O_2 and Anaerobic Oxidation. The nature of the inactive state formed under oxidizing conditions was further investigated, either when the electrode is poised at a high potential or upon exposure to oxygen. Figure 7A shows six chronoamperograms, recorded in experiments during which the enzyme was first oxidized under anaerobic conditions by stepping the electrode potential up (at $t = 0$ s) and then further inhibited by injecting an aliquot of solution saturated with O_2 in the electrochemical cell (at $t = 1000$ s). These chronoamperograms were successively recorded with the same enzyme film, after a short reactivation period at $E \approx -400$ mV (open circuit) preceding each potential step. No contribution from the capacitive current is seen in Figure 7A because the current was monitored after a 20 s equilibration period. Also, the contribution from the direct reduction of oxygen is negligible in the potential range used here.

We first focus on the first half ($t < 1000$ s) of each chronoamperogram (anaerobic inactivation). The dashed line overlaying the first part of the red chronoamperogram in the main panel of Figure 7A is an example of the perfect fit of each signal to:

$$i = (i_0 - i_\infty) \exp(-k_{inact}^{app} t) + i_\infty \quad (1)$$

The activity decreases exponentially toward a current i_∞ with an apparent time constant $1/k_{inact}^{app}$. The value of i_∞ depends on

(67) Luo, X. J.; Brugna, M.; Tron-Infossi, P.; Giudici-Orticoni, M. T.; Lojou, E. *J. Biol. Inorg. Chem.* **2009**, *14*, 1275–1288.
(68) Goldet, G.; Wait, A. F.; Cracknell, J. A.; Vincent, K. A.; Ludwig, M.; Lenz, O.; Friedrich, B.; Armstrong, F. A. *J. Am. Chem. Soc.* **2008**, *130*, 11106–11113.
(69) Vincent, K. A.; Cracknell, J. A.; Lenz, O.; Zebger, I.; Friedrich, B.; Armstrong, F. A. *Proc. Nat. Acad. Sci. U.S.A.* **2005**, *102*, 16951–16954.

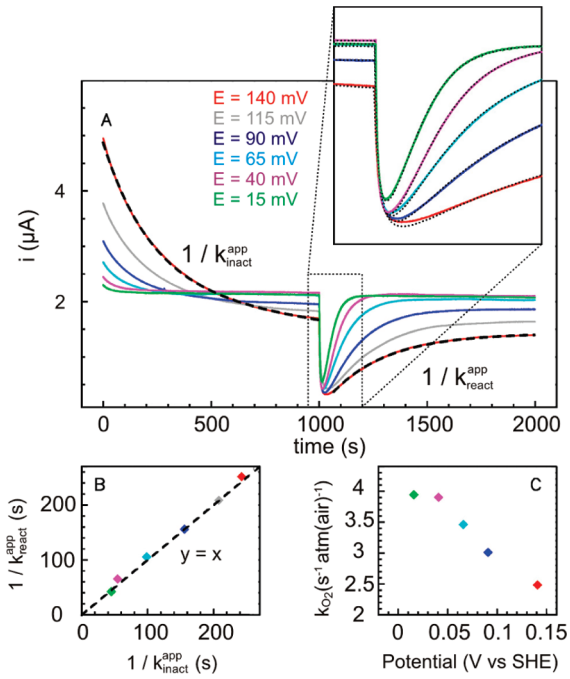

Figure 7. Anaerobic/aerobic inactivation and reactivation of *A. aeolicus* Hase I. (A) Chronoamperograms for the enzyme adsorbed on a graphite electrode and poised at various potentials. From $t = 0$ to $t = 1000$ s, the current decreases as a consequence of anaerobic inactivation. At $t = 1000$ s, an aliquot of O_2-saturated buffer is injected in the cell (final concentration 78 μM), and the recovery of activity is monitored. The dashed lines overlaying the red data are fits to exponential functions. In the inset, the dotted lines are the best fits of the data using eqs 2 and 4 (see text). (B) Time constant of the reactivation after exposure to O_2 plotted against the time constant of anaerobic inactivation; both were measured from fitting the relaxations to exponential functions (i.e., dashed lines overlaying the red chronoamperogram in A). (C) Bimolecular rate constant of aerobic inactivation as a function of electrode potential. Experimental conditions: pH 7, $T = 40$ °C, 1 bar H_2.

potential; this reveals that an equilibrium is reached between the active and the anaerobically inactive enzyme.

$$\text{active} \underset{k_a}{\overset{k_i}{\rightleftharpoons}} \text{inactive(anaerobic)} \qquad (2)$$

The enzyme activates or inactivates depending on the electrode potential (E) because k_i and/or k_a depend on E. When equilibrium is reached, the fraction of the enzyme in the active state equals $k_a/(k_i + k_a)$ and the relaxation rate is then given by

$$k_{\text{inact}}^{\text{app}} = k_i + k_a \qquad (3)$$

It is important to realize that the *apparent* rate constant of the exponential relaxation, at $t < 1000$ s in Figure 7, is equal to $k_i + k_a$ and not to k_i, a point which has been previously overlooked. Therefore, to avoid any ambiguity, we use the adjective "true" (as opposed to "apparent") to denote the (in)activation rate constants k_i and k_a. By fitting the anaerobic parts of the data (Figure 7A) to eq 1, we found that as the electrode potential increases from 15 to 140 mV the value of $k_{\text{inact}}^{\text{app}}$ decreases from 0.02 s^{-1} to about 0.004 s^{-1}.

At $t = 1000$ s (second part of the chronoamperograms), aliquots of O_2-saturated buffer were injected into the electrochemical cell solution to reach a final concentration of 78 μM. Anaerobicity was recovered with a characteristic time $\tau_{O2} \approx 15$ s by flushing H_2 in the electrochemical cell.[39] Figure 7A shows that after exposure to O_2, recovery of the activity is complete within 100−1000 s depending on potential. Thus, the relaxation rate of the current is not limited by O_2 release from the buffer. Moreover, as the electrode potential decreases the reactivation rate increases (as observed with the MBH enzyme from *R. eutropha*[69]), suggesting that the latter is conditioned by a redox process.

The apparent reactivation rate constants $k_{\text{react}}^{\text{app}}$ were measured by fitting the data to exponential functions (see e.g. the dashed line over second half of the red chronoamperogram in Figure 7A), and in Figure 7B $1/k_{\text{react}}^{\text{app}}$ was plotted as a function of $1/k_{\text{inact}}^{\text{app}}$. The key observation here is that all the data points fall on the line $y = x$. This shows that, at every potential, the rate at which activity is recovered after exposure to oxygen is the same as the apparent rate at which the enzyme is anaerobically inactivated. The fact that the *relaxation* after exposure to O_2 is complete and follows first order kinetics strongly suggests that a *single* inactive species has been formed upon exposure to O_2. When anaerobic conditions are restored, the equilibrium between active and inactive states relaxes at the same rate ($k_i + k_a$) as it does under oxidizing conditions in the absence of oxygen. Therefore, these two relaxation rates reveal the same equilibration process. We conclude that the mere effect of adding oxygen is to force the formation of the "anaerobic" inactive state (i.e., Ni-B), consistent with the finding of Armstrong and co-workers in ref 65. This contrasts with the observation that standard hydrogenases are oxidized to the Ni-B state under anaerobic conditions,[40] and to a mixture of Ni-A and Ni-B states under aerobic conditions.[39,21]

3.2.3. Kinetics of Reaction with O_2. The complete chronoamperograms in Figure 7A could be fitted by assuming that: (i) the active state is formed from the inactive state with a first order rate k_a, (ii) the potential-dependent pseudo first order rate for the formation of the inactive state equates k_i before the injection of O_2 and (iii) $k_i + k_{O2}[O_2]$ after the injection of O_2, where $k_{O2}[O_2] = k_{O2}[O_2]_0 \cdot \exp(-t/\tau_{O2})$; k_{O2} denotes the bimolecular rate constant for the formation of the inactive form upon reaction with O_2 and τ_{O2} is the relaxation time constant of the O_2-concentration in the electrochemical cell. Therefore, eq 2 applies at $t < 1000$ s, while at $t > 1000$ s it is replaced with

$$\text{active} \underset{k_a}{\overset{k_i + k_{O2}[O_2]_0 \exp(-t/\tau_{O2})}{\rightleftharpoons}} \text{inactive(anaerobic)} \qquad (4)$$

The term "$k_{O_2}[O_2]$" is responsible for the fast inhibition that follows the injection, and this rate of anaerobic inhibition decays exponentially as O_2 is flushed away by the stream of H_2. The protein films being very stable, there was no need to correct the data for film desorption.

The best fits of the chronoamperograms, shown with dotted lines in the inset of Figure 7A, were obtained by adjusting for each experiment the values of k_i, k_a, the current at time zero, k_{O_2} and τ_{O_2}. The first part of the experiment (before oxygen is added) leads to an unambiguous determination of k_i, k_a and the initial current. The second part of the data defines τ_{O2} (we found that it ranges from 13 to 15 s), and k_{O2} (the values of which are plotted in Figure 7C as a function of electrode potential). The very good agreement between the data and the model supports the hypothesis of bimolecular inhibition kinetics. This is in agreement with previous studies on standard hydrogenases for which the irreversible reaction with O_2 is also first order in $[O_2]$.[39] We note that *A. aeolicus* Hase I reacts about ten times

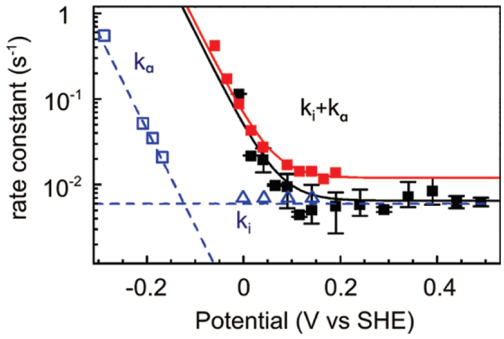

Figure 8. Dependence of the apparent rates of anaerobic inactivation and reactivation on electrode potential, determined by chronoamperometry experiments with *A. aeolicus* Hase I (filled symbols, this work) and *A. vinosum* hydrogenases (open symbols).[40] For *A. vinosum*, the rates of anaerobic (in)activation (open triangles) were obtained from data available in the literature[40] and the experimental conditions were pH 8.8, 45 °C. The dashed lines indicate the dependence on potential of the true rate constants k_i and k_a; only their sum can be determined by fitting the relaxation of the current after a potential step (see text). For *A. aeolicus* Hase I, the black and red squares represent experiments carried out under 1 and 0.1 bar H_2, respectively, at pH 7, 40 °C. Note the logarithmic *y* scale.

more slowly with O_2 than the standard hydrogenase from *D. fructosovorans*.[70]

Figure 7C shows that the rate of reaction of aerobic inhibition of *A. aeolicus* Hase exhibits a weak dependence on electrode potential, as noted previously for the enzyme from *R. eutropha*.[69] This is unlike the case of the *D. fructosovorans* enzyme, whose rate of reaction with O_2 is potential-independent in the range 50-500 mV (Figure 9 in ref 39).

3.2.4. Anaerobic (In)Activation of Hase I. Figure 8 shows the apparent rates of (in)activation for the *A. aeolicus* Hase I (filled squares). These were determined by fitting the exponential relaxations of the current recorded after stepping up or down the electrode potential (to force an oxidative inactivation or reactivation, respectively). This relation between rates and driving force can yield valuable information on the (in)activation mechanism, as shown for the oxygen-sensitive hydrogenase from *A. vinosum*.[40]

For comparison, Figure 8 shows also the dependence on the potential of the apparent rates of (in)activation obtained with *A. vinosum* hydrogenase, plotted as blue, empty symbols, replotted from the data in ref 40, and fitted to straight lines. These *apparent* rates were measured by fitting current transients to exponential functions, and interpreted as the *true* constants k_i and k_a, respectively (see eqs 2 and 3). In this case, this was a good approximation because these rates were determined under conditions where the relaxation is essentially irreversible (either at high potential, where $k_i \gg k_a$ and therefore $k^{app} \approx k_i$, or at low potential where $k_a \gg k_i$ and $k^{app} \approx k_a$). The rate of reductive activation for the *A. vinosum* enzyme is potential dependent; whereas the rate of inactivation is not.

For the *A. aeolicus* Hase I, the apparent rate of interconversion between active and inactive states also increases exponentially as the potential is lowered (because k_a increases and k_i is constant). At high potentials, the apparent rate of oxidative inactivation becomes constant as k_a becomes lower than k_i. Clearly, the dependence of the (in)activation rate constants on potential is the same for *A. aeolicus* and *A. vinosum*, which strongly suggests that in both enzymes the mechanism of formation of Ni-B is similar.[73]

In the same figure the effect of the H_2 concentration on the rates of (in)activation is also illustrated. A comparison between data obtained with *A. aeolicus* Hase I at pH 7 under 1 bar H_2 (black) and 0.1 bar H_2 (red), respectively, demonstrates that the true rate of inactivation (k_i) decreases when the concentration of H_2 increases. Therefore, H_2 protects the *A. aeolicus* Hase I against anaerobic oxidation, like it does in the case of the standard hydrogenases from *A. vinosum*[40] and *D. gigas*.[37]

4. Discussion

The Hase I from *A. aeolicus* is an exceptional enzyme that exhibits thermostability and high oxygen-resistance. It is thus compelling to elucidate the mechanism associated with the function of this enzyme and to identify what determines its intriguing properties.

4.1. Active Site Coordination. In this study we have presented the first comprehensive FTIR investigation of a [NiFe] hydrogenase from a hyperthermophilic, oxygen-tolerant bacterium, namely *A. aeolicus*. The active site of this enzyme is found to retain the iron coordination of one carbonyl and two cyanide ligands typical for standard hydrogenases. This agrees with recent observations on the oxygen-tolerant MBH from *R. eutropha*,[45] but not with those on the soluble NAD^+-reducing hydrogenase (SH) from the same organism, in which additional CN^- ligands were proposed to coordinate both nickel and iron.[44,71] Clearly, the oxygen tolerance of *A. aeolicus* Hase I is not related to the presence of additional diatomic ligands in its active site.

4.2. Spectroscopic Signatures of the Inactive Oxidized Enzyme; the "Ready" Ni-B State. The FTIR spectrum of the as-isolated Hase I showed absorption bands of an oxidized state, which on the basis of concomitant EPR studies (Figure 3) can be assigned to Ni-B (see also ref 13). The Ni-A state observed in all oxygen-sensitive hydrogenases is absent in *A. aeolicus*. The g-values corresponding to the Ni-B state are slightly different from those of standard hydrogenases[23] with the largest deviation being observed for the g_x component (Table S1). The IR stretching vibrations of the CN^- ligands are very similar while those of CO show small but more pronounced deviations from those of Ni-B present in oxygen-sensitive hydrogenases (Table 1 and S2, Supporting Information). This is as anticipated, since CO is more sensitive to electronic changes than the cyanide ligands, which are in addition hydrogen-bonded to neighboring amino acid residues.[60] Furthermore, a sequence comparison showed a difference in the amino acid residues in the vicinity of the CO ligand (e.g., Ser67, Ile68 in *A. aeolicus* that correspond to Tyr70 and Val71 in the standard hydrogenase from *D. fructosovorans*) that is also expected to contribute to these small deviations in the CO stretching vibrations. These data indicate that the structure of the active sites is rather similar in both types of hydrogenases. X-ray crystallographic and EPR/ENDOR[22] studies on the *D. vulgaris* Miyazaki F hydrogenase have detected a hydroxide ligand bridging the two metal ions in this state, rendering it inactive. It is proposed that such an oxygenic species coordinates also the [NiFe] site in *A. aeolicus* Hase I, suggesting that the latter has the affinity of binding an oxygen-based ligand. Ni-B represents an inhibited form that is, however, quickly activated.

4.3. Inactive Oxidized Enzyme; Aerobic and Anaerobic Inactivation. The protein film electrochemistry (PFE) experiments in Figure 7 demonstrate that the same inactive product

(70) Two to 4 $s^{-1}(atm(O_2))^{-1}$ at 40 °C, pH 7, versus 40 $s^{-1}(atm(O_2))^{-1}$ in ref 39.

(71) van der Linden, E.; Burgdorf, T.; Bernhard, M.; Bleijlevens, B.; Friedrich, B.; Albracht, S. P. J. *J. Biol. Inorg. Chem.* **2004**, *9*, 616–626.

is formed when the enzyme is oxidized either directly by oxygen or using an oxidizing potential under anaerobic conditions (cf the discussion of Figure 7B). Figure 7A also shows that the *relaxation* of the inactivation process after exposure to O_2 is complete and follows first-order kinetics. This strongly suggests that a *single* inactive species is formed in this process. In addition, results from FTIR and EPR show that both the anaerobically oxidized and the aerobically prepared enzymes are in the Ni-B state (the Ni-A and Ni-SU states could not be detected). Thus, the reaction of the *A. aeolicus* Hase I with O_2 forms explicitly the Ni-B state that is the same inactive species as that produced when the enzyme is oxidized under anaerobic conditions. This is consistent with the findings of Armstrong and co-workers in ref 65 for the oxygen-tolerant MBH enzyme from *R. eutropha*, but different from those obtained for standard hydrogenases. The latter are oxidized to the Ni-B state under anaerobic conditions, and to a mixture of Ni-A and Ni-B in the presence of O_2.[21,39] The important difference between *A. aeolicus* and standard hydrogenases is that the former reacts with O_2 to form a single species, which is reactivated at a much faster rate than in standard hydrogenases (Figure 8).

The fact that Ni-B, the product of the reaction of the enzyme with O_2, is formed also under anaerobic conditions-using a high electrode potential alone or chemical oxidants-should not be taken as an indication that O_2 does not reach the active site. Indeed, the electrochemical data suggest otherwise. When the Ni-B state is formed either directly on the electrode or by chemical oxidation, the distal [FeS] cluster mediates the oxidation of the active site. A key observation is that the apparent rate of inactivation ($k_{app} \approx k_i$, Figure 8) is independent of electrode potential above 150 mV, suggesting that the anaerobic formation of Ni-B is limited by a chemical step.[40] When the conditions become aerobic (e.g., at $t = 1000$ s in Figure 7), the oxidation of the distal [FeS] cluster provides an additional driving force for the mediated oxidation of the active site, but this should not increase the rate of inactivation, which is limited by a chemical step (i.e., incorporation of an oxygenic ligand) that precedes its oxidation.[40] Hence the observation in Figures 6 and 7 that adding oxygen does increase the rate of inactivation, strongly suggests that it involves direct attack of O_2 at the [NiFe] center, rather than an oxidation of the active site that would be mediated by the [FeS] clusters.

4.4. Transition to the Active Enzyme; the EPR-Silent Ni-SI_a State. The one-electron reduction of Ni-B in the Moss cell leads to the appearance of an EPR-silent state with a CO stretching vibration at 1927 and CN^- stretching vibrations at 2077 and 2087 cm^{-1}. On the basis of its infrared spectrum, the reduced species in Figure 2b is associated with Ni-SI_a rather than with (Ni-SI_r)$_I$. We consider it less likely that it corresponds to a transient species (Ni-SI_r)$_{II}$, reported to have infrared stretching vibrations[27] identical to Ni-SI_a.[27,64,72] At ambient temperatures (i.e., at 25 °C or above), the putative water ligand in (Ni-SI_r)$_{II}$ is rapidly released and transition to Ni-SI_a is thermodynamically favored. Indeed when titrations are performed at 4 °C, and in particular when H_2 reduced enzyme is left for long times at this temperature, small but consistent shifts in the IR bands are observed, which may arise from transition of the "active" Ni-SI_a to the inactive (Ni-SI_r)$_{II}$. The state described by the FTIR spectrum in Figure 2b is thus assigned to Ni-SI_a. Reoxidation of the sample to Ni-B at lower temperatures (4 °C), where the inactivation kinetics becomes markedly slower[26,27] did not yield new spectroscopic features, that is, (Ni-SI_r)$_I$. A change of the pH of the solution did not lead to a detectable appearance of the (Ni-SI_r)$_I$ state either.[34]

The results of our protein film electrochemistry experiments show that the mechanism of formation of Ni-B under anaerobic conditions resembles that in standard hydrogenases. The potential-dependence of the rates for the Ni-B state formation/reactivation (Figure 8) in *A. aeolicus* Hase I follows the same pattern as for the *A. vinosum* hydrogenase: the rate of anaerobic oxidation (k_i) is independent of potential, whereas the rate of reductive activation (k_a) increases exponentially as the potential becomes more negative. This appears to indicate that the rate of inactivation depends on a chemical step that is followed by an oxidation, whereas reactivation is triggered by an electron transfer.[40,73] Although the rate of inactivation is similar in *A. vinosum* and *A. aeolicus*, there is a 200-fold difference in the rate of reactivation of the *A. aeolicus* enzyme compared to that of *A. vinosum* (at a given electrode potential). We propose that this is a result of the inactive Ni-SI_r species being highly reactive (absent in the IR-spectroelectrochemistry) leading to the fast transition of Ni-B to the active state of the enzyme.

The redox potential for the Ni-B/Ni-SI_a couple obtained from IR spectroelectrochemistry is equal to -105 ± 10 mV. This value cannot be directly compared to those measured for the oxygen sensitive enzymes, since in *A. aeolicus* the inactive (Ni-SI_r)$_I$ could not be detected. However, we note that it is only 30−50 mV more positive than the values reported for *D. gigas*[26] (−135 mV, pH 7.7), *A. vinosum*[27] (−140 mV, pH 7.4) and *D. vulgaris*[26,34] (−151 mV, pH 7.4). Clearly, the value of the electrode potential at which the enzyme reactivates in cyclic voltammetry experiments (the parameter E_{sw} in Figure 5) is not directly related to a thermodynamic parameter such as the redox potential potential of the Ni-B/Ni-SI_a couple. This shows that the value of the E_{sw} is an empirical quantity that is not equal to the reduction potential of Ni-B. The very positive E_{sw} value found in *A. aeolicus* Hase I, which is indicative of O_2-tolerance,[74] is thus proposed to result from the fact that the reactivation is very fast and not from the fact that the reduction potential of the Ni-B state is very high. The relation between rate of (in)activation and voltammetric signature is studied in detail in ref 73.

4.5. Central States in the Catalytic Mechanism; Ni-C and Ni-R. Further reduction of Ni-SI_a is followed by the appearance of signals at higher frequencies, with the CO band centered at 1949 cm^{-1} and the coupled CN^- pair at 2078 and 2088 cm^{-1}, respectively. These signals correspond to the Ni-C state. In agreement with standard hydrogenases the CN^- bands of Ni-SI_a and Ni-C are very similar. The titrations at pH 7.4 exhibited a comparatively small yield of the Ni-C state, while at higher pH (8.4) it could not even be discerned as a detectable intermediate. ENDOR and HYSCORE studies on the Ni-C state in *A. aeolicus* have detected also a hydride ligand at its active site as previously reported for the regulatory hydrogenase from *R. eutropha* and the standard hydrogenase from *D. vulgaris* Miyazaki F.[28,29,75] However, in the case of the *A. aeolicus* Hase I this hydride was found to be more loosely bound,[75] in line with the substoichiometric yield of the Ni-C state in the IR

(72) George, S. J.; Kurkin, S.; Thorneley, R. N. F.; Albracht, S. P. J. *Biochemistry* **2004**, *43*, 6808–6819.

(73) Fourmond, V.; Infossi, P.; Giudici-Orticoni, M. T.; Bertrand, P.; Léger, C. *J. Am. Chem. Soc.* **2010**, *132*, 4848–4857.

(74) Cracknell, J. A.; Vincent, K. A.; Ludwig, M.; Lenz, O.; Friedrich, B.; Armstrong, F. A. *J. Am. Chem. Soc.* **2008**, *130*, 424–425.

(75) Pandelia, M.-E. Doctoral Thesis, Technical University Berlin, Germany, 2009.

titrations and its complete absence at pH 8.4, which indicates an increased instability of the hydride complex under more alkaline conditions.

At a potential of −444 mV at pH 7.4 all redox processes are completed and the enzyme is found in the most reduced Ni-R state with the FTIR bands shifted to lower frequencies, suggesting an increase in the electron density at the Fe. There are no signals corresponding to Ni-C, which shows that at 25 °C there is no detectable turnover of the enzyme (hydrogen production) that would lead to an equilibrium between Ni-C and Ni-R states, as occurs in standard hydrogenases.[27]

The exact coordination of the active site of the Ni-R state has not yet been characterized for the mesophilic hydrogenases. It is considered to retain the hydride ligand that would stabilize this EPR-silent complex and ensure a fast, reversible catalysis.[76,77] Depending on pH, there are three such states formed—Ni-R1, Ni-R2 and Ni-R3—which correspond to different degrees of protonation of the active site.[26,27,34] However, in *A. aeolicus* Hase I, only one Ni-R could be detected, which is spectroscopically similar to Ni-R2 (or Ni-R3) and not to the typical Ni-R1 form expected at physiological pH (Table 1 and S2, Supporting Information). In standard hydrogenases, Ni-R2 shows considerable intensity only at high pH values,[27] at which the observed turnover of these enzymes decreases. The most reduced state of Hase I is thus associated with the so-called Ni-R2, which might represent a deprotonated form of this species.

The midpoint potential for the Ni-SI_a/Ni-C couple is −295 mV and for the Ni-C/Ni-R couple −300 mV. These values are approximately 70−140 mV more positive than the respective potentials measured in mesophilic anaerobic hydrogenases;[26,27,34] this appears to correlate with the fact that the *A. aeolicus* enzyme is tuned to operate in the oxidative direction. We also note that H_2 oxidation occurs at an electrode potential that is significantly above the reduction potential of the H^+/H_2 couple (Figure 5). This is like in the MBH from *R. eutropha*,[68] and unlike in standard hydrogenases: the latter oxidize H_2 under reversible conditions.[39,78] We propose that the overpotential for the oxidation of H_2 is a consequence of the reduction potential of the Ni-SI_a/Ni-C and Ni-C/Ni-R couple being upshifted with respect to standard hydrogenases. This should contribute to make *A. aeolicus* Hase I a better catalyst of H_2 oxidation than production. Experiments carried out on the Hase I-cyt*b* complex and the Hase I (without cyt*b*) led to essentially identical results, showing that the presence of cyt*b* does not shift the redox potentials of the various intermediates. A summary of the observed states and the redox potentials determined for the related transitions is given in Scheme 2. Similar to standard hydrogenases this enzyme cycles between Ni-SI_a, Ni-C and Ni-R states. However, these redox events occur at higher potentials.

4.6. pH Dependence of the Redox Transitions. All the midpoint potentials measured in the present work are pH dependent in the pH range examined between 6.4 and 8.4. The pH dependence is smaller than that predicted for a proton transfer coupled to an electron transfer (−59 mV/pH at 25 °C) and this finding is consistent with titrations in oxygen sensitive hydrogenases from the *Desulfovibrio* and the *Allochromatium* species and may indicate that the pK_a value of a nearby amino-

Scheme 2. Schematic Overview of the Proposed Catalytic Cycle for the Hase I from the Hyperthermophilic Bacterium *A. aeolicus*[a]

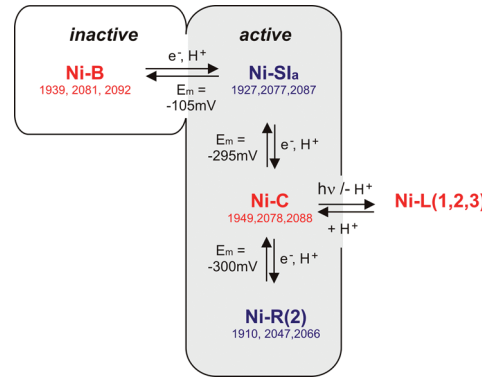

[a] Paramagnetic states are denoted in red and the EPR-silent states in blue. The infrared stretching vibrations at 25 °C are also included. The midpoint potentials for these redox transitions are given for pH 7.4.

acid is affected by reduction of the redox center. In a spectroelectrochemical study of the *D. vulgaris* Miyazaki F hydrogenase the amino acid residue responsible for this deviation of the pH-dependent potentials was proposed to be one of the ligating cysteinyl residues of the nickel metal ion.[34] A subsequent characterization of site-directed mutants may serve to identify the residues responsible for this effect.

4.7. Oxygen Tolerance of Hase I. The PFE experiments presented in this work clearly show that *A. aeolicus* Hase I behaves like the oxygen tolerant [NiFe] hydrogenases (MBH from *R. eutropha* and Hyd-1 from *E. coli*),[66,68] and unlike the standard hydrogenases from *A. vinosum*, *D. gigas*, *D. fructosovorans* and *E. coli* (Hyd-2). *A. aeolicus* Hase I requires only mild reducing conditions to reactivate after anaerobic inactivation (E_{sw} is high, Figure 5), and inhibition by O_2 is fully reversible. As an example, at +210 mV (pH 7), simply removing the oxygen is enough to reactivate the *A. aeolicus* enzyme (Figure 6), whereas reactivation of standard hydrogenases can occur only after their reduction below approximately −120 mV.[40]

Armstrong and co-workers have proposed that oxygen tolerance may be a consequence of (i) oxygen access to the active site being slow, (ii) the reaction of O_2 being selective for the formation of an inactive state that is easily reactivated, and/or (iii) reactivation being fast.[79] Within the framework of our present results, these hypotheses can now be examined.

Recently, it was shown that slowing oxygen access to the active site of standard [NiFe] hydrogenases decreases the rate of inhibition by O_2 under the condition that the rate of intramolecular transport is slower than the reaction of O_2 at the active site.[55] This is the case in certain mutants of the *D. fructosovorans* hydrogenase, but not for the wild type enzyme. The rate of the reaction of *A. aeolicus* Hase I with O_2 (Figure 7C) is about 10 times slower than in the wild type *D. fructosovorans* hydrogenase, but this does not necessarily imply that oxygen transport is slower. In ref 55, a two-step model has been used to interpret oxygen inhibition kinetics, whereby the formation of a geminate state precedes the reaction of O_2 at the active site. In this work, the second order rate constant of O_2 access to the active site is denoted by k_1, the first order rate constant of O_2 release by k_{-1}, and the first order rate constant of the chemical reaction by k_2.

(76) Volbeda, A.; Fontecilla-Camps, J. C. *Bioorganomet. Chem.* **2006**, *17*, 57–82.
(77) Fontecilla-Camps, J. C.; Amara, P.; Cavazza, C.; Nicolet, Y.; Volbeda, A. *Nature* **2009**, *460*, 814–822.
(78) Pershad, H. R.; Duff, J. L. C.; Heering, H. A.; Duin, E. C.; Albracht, S. P. J.; Armstrong, F. A. *Biochemistry* **1999**, *38*, 8992–8999.
(79) Armstrong, F. A. *Photosynth. Res.* **2009**, *102*, 541–550.

Within this framework, the bimolecular rate constant of inhibition that we determined by fitting chronoamperometry experiments (Figure 7C) is equal to k_2k_1/k_{-1} and its dependence on potential (Figure 7C) most likely reveals that of k_2. The difference between the bimolecular rates of inhibition in *A. aeolicus* and *D. fructosovorans* is not conclusive because it may result from any of these three rate constants being different.

However, in support of hypothesis (ii), reaction of O_2 at the active site of *A. aeolicus* Hase yields only the Ni-B state, which reactivates more quickly than Ni-A. Under similar conditions, the standard hydrogenases are oxidized into a mixture of Ni-B and Ni-A states.[21,39] The molecular determinant for the selectivity of *A. aeolicus* Hase I cannot yet be ascertained. By aligning the amino acid sequences of standard and oxygen tolerant [NiFe] hydrogenases, Ludwig et al. found that the residues at approximately 10 Å around the [NiFe] active site are highly conserved.[9] The formation of the oxidized inactive states upon partial reduction of oxygen at the active site requires both electrons and protons. The rates of proton transfer are so strongly dependent on distance[80] that the exact position (not only the nature) of the lateral chains of the amino acids surrounding the active site must strongly affect the inactivation kinetics. This may also affect selectivity (formation of Ni-A versus Ni-B) if the protons used to make Ni-A and Ni-B do not take the same paths.

Hypothesis (iii) also explains in part the oxygen tolerance of *A. aeolicus*: Figure 8 demonstrates that at a given electrode potential, the reactivation of the Ni-B state is more than 2 orders of magnitude faster in *A. aeolicus* than in *A. vinosum*. We can exclude that reactivation of Ni-B is fast *because* the structure of the substrate channels favors the diffusion of the hydroxo ligand to the solvent: if this diffusion step determined the rate of reactivation, the latter would not depend on potential; in contrast, Figure 8 clearly shows that the rate of reactivation is determined by an electron transfer step. We could also rule out the hypothesis according to which the reactivation is fast because the reduction potential of Ni-B is high. We speculate that the fast reactivation results from the fact that the interaction of the oxygenic ligand with the [NiFe] site in *A. aeolicus* is weak. This is supported by the changes in the EPR spectrum of Ni-B[13] indicating a slightly different electronic structure of the spin carrying [NiFe] center. We also note that since the reduction of Ni-B requires one proton,[40] its rate is likely to be strongly dependent on the exact position of the amino acids that surround the nickel.

5. Conclusions

The present study is the first combined spectroscopic and electrochemical investigation of an oxygen tolerant, hyperthermophilic hydrogenase. Our aim was to characterize its redox chemistry, gain insight into activation/inactivation mechanisms and study the mechanism of oxygen inhibition.

Not all redox states known from other hydrogenases were observed in *A. aeolicus*. Only four redox intermediates of this enzyme could be detected and characterized; one inactive state that corresponds to the "ready" Ni-B state and three catalytically active states assigned to Ni-SI_a, Ni-C and Ni-R, respectively. The "unready" inactive Ni-A and Ni-SU states were not observed, a finding that agrees with results obtained on the oxygen-tolerant MBH from *R. eutropha*.[45] Furthermore, $(Ni\text{-}SI_r)_I$ could not be resolved as an intermediate in the transition from Ni-B to the active enzyme. This may indicate that the pK_a of the amino acids that are responsible for the acid base transitions are different. These are yet to be identified, e.g. by mutagenesis experiments. It is interesting that only one Ni-R state is observed in *A. aeolicus*, which contrasts the results found for standard hydrogenases. The reduction potentials of the Ni-SI_a/Ni-C and Ni-C/Ni-R transitions lie approximately 100 mV higher than those of standard hydrogenases. This is consistent with the observation in PFE that the catalytic wave is shifted up. This also explains that the enzyme is much better at oxidizing H_2 than at producing it. Hase I from *A. aeolicus* is oxygen tolerant. It fully recovers activity after O_2 is flushed away; this is the same phenotype as that of the membrane bound hydrogenase from *R. eutropha.*

Based on protein film electrochemical and spectroscopic data it is clearly shown that the transient species that is formed upon exposure to O_2 is Ni-B; the same state is formed upon electrochemical or chemical oxidation under anaerobic conditions. The reduction potential of Ni-B is not much larger than that in standard hydrogenases. Therefore the shift in the voltammetric "switch potential" E_{sw} is not due to the reduction potential of Ni-B being greater. From a kinetic point of view, the mechanism of anaerobic formation and reactivation of Ni-B as appears to be similar to that in standard hydrogenases, for example, *A. vinosum.* This is further discussed in ref 73. The rate of inactivation is the same, but the rate of reactivation is more than 2 orders of magnitude larger, despite the fact that the reduction of Ni-B is not more favorable than in standard hydrogenases. This contrasts with the hypothesis in refs 65 and 66 that the reduction of the Ni-B state is thermodynamically favored in oxygen tolerant hydrogenases. The fast reactivation of Ni-B is the main difference between the oxygen tolerant and the oxygen sensitive enzymes. The electrochemistry data support the hypothesis that O_2 inhibits the enzyme by reacting at the [NiFe] center (rather than at a surface exposed center); a definite conclusion is expected from results of EPR measurements using ^{17}O labeled water or dioxygen.

Further questions to be solved in future experiments, in addition to the mechanism of O_2 attack at the active site and the interaction with other potential inhibitors like carbon monoxide, are (i) the reason for the Ni-A state not being formed, (ii) the detailed geometry associated with the low yield of Ni-C; (iii) the structure of the Ni-R state and (iv) the electron and proton transfer events to the active site, which play a role in the generation of the various intermediates and determine the activity of the enzyme. Although many details of these intermediates are now known, a final picture has not been evolved.

The hydrogenase from the hyperthermophilic bacterium *A. aeolicus* is shown to be an ideally designed system and is thus highly interesting for biotechnological applications.[8,67] It is stable at very high temperatures, it can be tightly attached to electrode surfaces and it is oxygen tolerant. The optimum function and enhanced oxygen tolerance of the Hase I from *A. aeolicus* is most likely related to a weaker bonding interaction with exogenous nonprotein ligands and to details of both proton and electron transfer processes. In this context the reduction potentials of the iron sulfur clusters need to be determined; this is currently under way in our laboratories.

(80) Bertrand, P. *J. Biol. Inorg. Chem.* **2004**, *9*, 2–11.

Acknowledgment. Leslie J. Currell is acknowledged for his technical support in the FTIR experiments. Birgit Deckers is particularly thanked for her help with the graphical artwork. This work was financially supported by the EU/Energy Network project SOLAR-H2 (FP7 contract 212508), BMBF (03SF0318B, 03SF0355C), the Max Planck Society, the CNRS, ANR, the city of Marseilles, Région Provence-Alpes-Côte d'Azur, and supported by the "Pôle de compétitivité CapEnergies".

Supporting Information Available: Supplementary Figures, control experiments for the protein film (PFE) electrochemistry measurements, comparative tables of FTIR and EPR spectral data, as well as a detailed description of the procedure for analyzing the infrared electrochemical titrations. This material is available free of charge via the Internet at http://pubs.acs.org.

JA910838D

The Membrane-Bound Hydrogenase I from the Hyperthermophilic Bacterium *Aquifex aeolicus*: Enzyme Activation, Redox Intermediates and Oxygen Tolerance

Supporting Information

Maria-Eirini Pandelia†[§], Vincent Fourmond[‡ §], Pascale Tron-Infossi[‡], Elisabeth Lojou[‡], Patrick Bertrand[‡], Christophe Léger[‡], Marie-Thérèse Giudici-Orticoni[‡], and Wolfgang Lubitz†[*]

†*Max-Planck-Institut für Bioanorganische Chemie, Stiftstrasse 34-36, D45470, Mülheim a.d. Ruhr, Germany*

[‡]*Laboratoire de Bioénergétique et Ingénierie des Protéines, IMM-CNRS, 13402 Marseille, France*

E-mail: lubitz@mpi-muelheim.mpg.de

Table S1. Comparison between the principal g-values corresponding to the EPR-detectable intermediates in Hase I from *Aquifex aeolicus*, MBH from *Ralstonia eutropha*, membrane attached [NiFe] enzyme from *Desulfovibrio vulgaris* Miyazaki F.

	A. aeolicus (Hase I)			*R. eutropha* (MBH)			*D. vulgaris* MF		
State	g_x	g_y	g_z	g_x	g_y	g_z	g_x	g_y	g_z
Ni-A	nd	nd	nd	nd	nd	nd	2.32	2.24	2.01
Ni-B	2.30	2.17	2.01	2.30	2.17	2.01	2.33	2.16	2.01
Ni-C	2.21	2.15	2.01	2.20	2.14	2.01	2.20	2.14	2.01
Ni-L	2.28	2.12	2.05	2.27	2.11	2.05	2.30	2.12	2.05
Ni-X	2.24	2.19	2.01	nd	nd	nd	nd	nd	nd

Table S2. Comparison of the infrared frequencies (cm^{-1}) corresponding to the stretching vibrations of the CO and CN^- ligands bound to Fe at 25 °C for the [NiFe] hydrogenases from: *Aquifex aeolicus* (Hase I), *Desulfovibrio vulgaris* Miyazaki F, *Allochromatium vinosum* and *Ralstonia eutropha* (MBH).

redox state	*A. aeolicus* (Hase I)		*D. vulgaris*[a] Miyazaki F		*A. vinosum*[b]		*R. eutropha*[c] (MBH)	
	$\bar{\nu}$ (CO)	$\bar{\nu}$ (CN)	$\bar{\nu}$ (CO)	$\bar{\nu}$ (CN)	$\bar{\nu}$ (CO)	$\bar{\nu}$ (CN)	$\bar{\nu}$ (CO)	$\bar{\nu}$ (CN)
Ni-A	-	-	1956	2085, 2094	1945	2082, 2093	-	-
Ni-B	1939	2081, 2092	1954	2081, 2090	1943	2079, 2090	1948	2081, 2098
Ni-SU	-	-	1958	2089, 2100	1948	2088, 2100	1942	2082, 2104
$(Ni\text{-}SI_r)_I$	-	-	1922	2061, 2070	1910	2052, 2067	1910	2055, 2063
$(Ni\text{-}SI_r)_{II}$	-	-	1943	2074, 2086	1931	2073, 2084	1936	2075, 2093
$Ni\text{-}SI_a$	1927	2077, 2087	1943	2074, 2086	1931	2073, 2084	1936	2075, 2093
Ni-C	1949	2078, 2088	1961	2074, 2085	1951	2073, 2085	1957	2075, 2097
Ni-R1	-	-	1948	2061, 2074	1936	2059, 2072	1948	2068, 2087
Ni-R2	1910	2047, 2066	1932	2051, 2065	1921	2048, 2064	1930	2049, 2075
Ni-R3	-	-	1911	2045, 2061	1913	2043, 2058	1919	2046, 2071

[a] Taken from reference [1]
[b] Taken from reference [2]
[c] Taken from reference [3]

Figure S1. Control experiment showing that the decrease of H_2-oxidation current that results from the dilution in H_2 concentration when 500µL of buffer saturated with N_2 (instead of 200 µL of buffer saturated with O_2 for the experiment in Figure 8 in the main text) is injected, at t = 100s, in the 3 mL cell solution, at pH 7, 40°C, under 1 atm H_2. Electrode rotation rate 3 krpm.

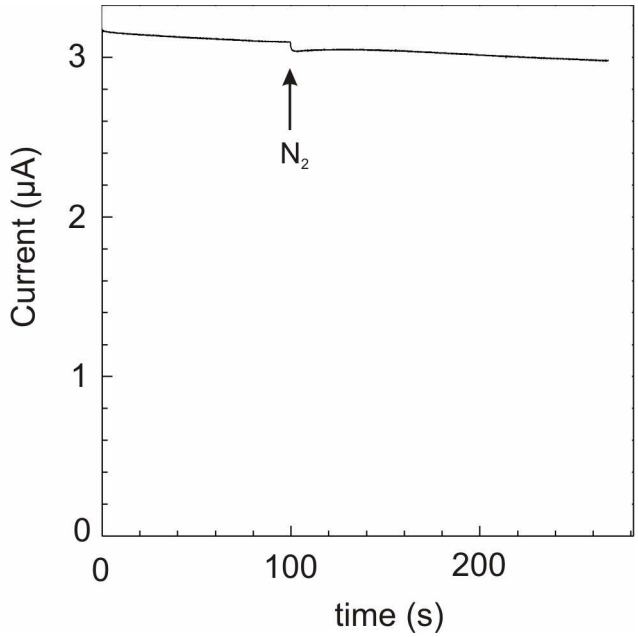

Figure S2. FTIR spectra of the Hase I - cyt*b* complex reduced for 40 min with H_2 and transferred into the IR cell under anaerobic conditions at 25°C (blue trace) and after 4 hours at 4°C (red trace). At 4 °C the FTIR bands corresponding to the Ni-SI_a state of the enzyme start to shift towards higher wavenumbers and the changes are complete after a waiting time of 4 hours. This behavior is reversible (upon heating up the sample to 25 °C), it is observed only for this state and has been related to the formation of the inactive EPR-silent $(Ni\text{-}SI_r)_{II}$ intermediate that has been proposed to carry a loosely bound water ligand. Experimental conditions: resolution 1cm^{-1}, 15.000 averages.

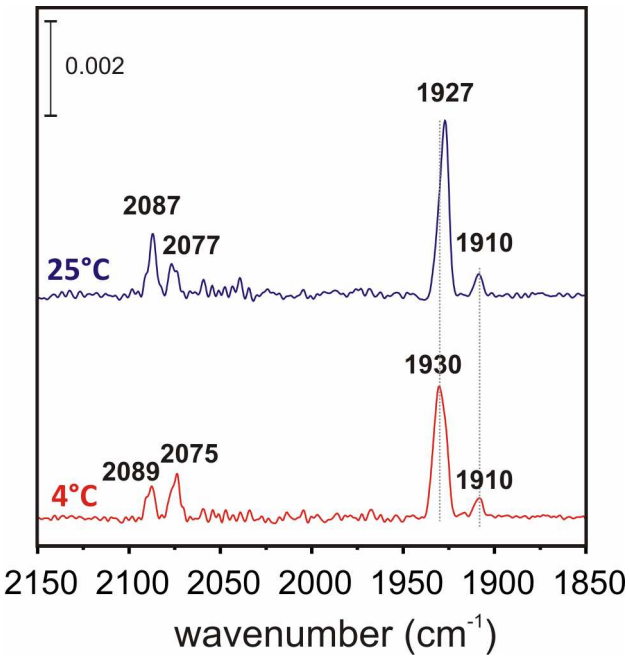

Figure S3. X-band cw EPR spectra of the as isolated Hase I-cyt*b* at 10 K (red) and 40 K (blue). Experimental conditions: mw frequency 9.45567 GHz, modulation amplitude 1 mT, mw power 2 mW, sample concentration 120µM.

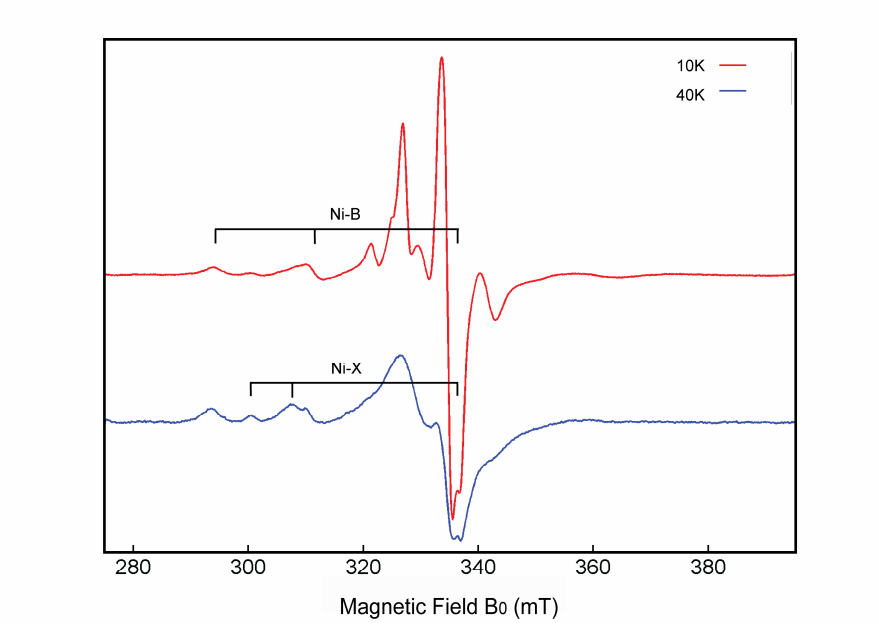

From Figure S3 the principal values of the g-tensor of the Ni-B state are determined to be $g_x = 2.30$, $g_y = 2.17$ and $g_z = 2.01$. Additional signals in the nickel region are present at g = 2.24, g = 2.19. These can be better discerned by increasing the temperature from 10 to 40 K. Interestingly, these additional signals disappear from the spectrum if the enzyme is preheated to 70°C (343 K) under aerobic conditions. The residual spectrum is a 'pure' Ni-B state (see Figure 3 and subsection 3.1.3. of the present manuscript).

The additional signal present in the as isolated enzyme could be better separated and further characterized by measurements at Q-band microwave frequencies (at ~34 GHz). It should be noted that the exact composition and type of the [FeS] clusters in *A. aeolicus* Hase I have not been identified so far. However, in the as-isolated enzyme the [FeS] cluster proximal to the [NiFe] centre is paramagnetic, resulting in a magnetic coupling of these two EPR-detectable species. Therefore the nickel signals in the Ni-B state, depending on the microwave frequency the experiment is carried out, appear broadened or 'split'[4] due to the spin-spin interaction with the so far not characterized EPR-active proximal [FeS] cluster.

Figure S4. 2 pulse-echo detected EPR spectra were recorded in the range of temperatures between 10 and 30 K. Experimental conditions: $\pi/2$ = 36 ns, tau = 330 ns, mw frequency 33.97635 GHz, shot rep. time 0.6 ms, sample concentration 120 µM.

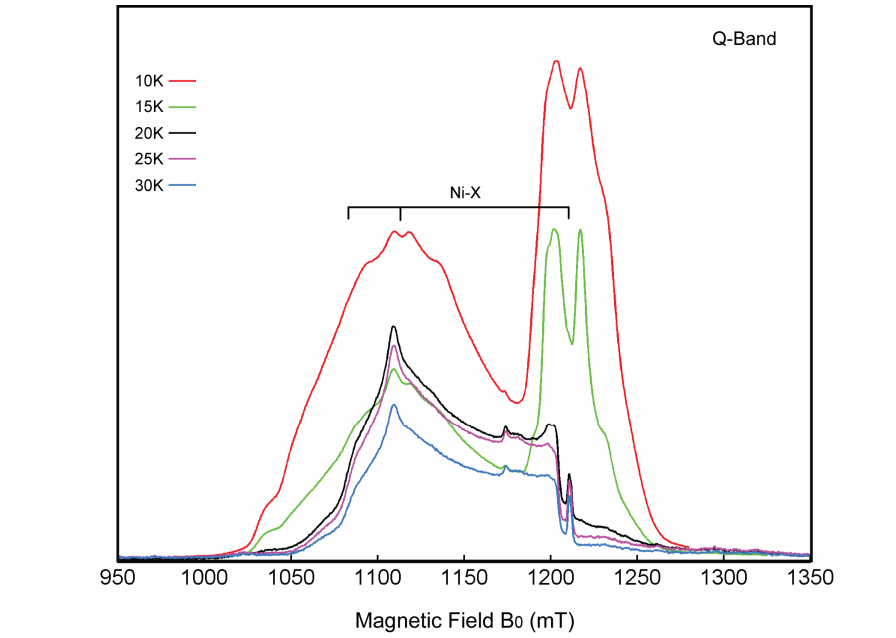

In Figure S4 at 30 K contributions from signals corresponding to Ni-B and the [FeS] centers disappear due to the different relaxation of this magnetically coupled system. The remaining signals correspond to the additional state present in the measurements at X-band frequencies (see Figure S2 or Figure 3 in the manuscript) that can now be completely characterized. The principal values of the g-tensor of this state are g_x = 2.24, g_y = 2.19 and g_z = 2.01 and are consistent with the signals in the X-band measurements. This state is denoted as Ni-X (see subsection 3.1.3. of the manuscript).

Most probably it is related to a [NiFe] state, conformationally different from Ni-B, which in addition does not magnetically interact with a [FeS] center.

Figure S5. FTIR spectra of the most reduced Ni-R state of the Hase I-cyt*b* from *A. aeolicus* at 25 °C. (a) pH 6.4 poised at -400 mV, (b) pH 7.4 poised at -444 mV and (c) pH 8.4 poised at -486 mV. No additional Ni-R forms were found to be in an acid-base equilibrium with this state in the pH range examined.

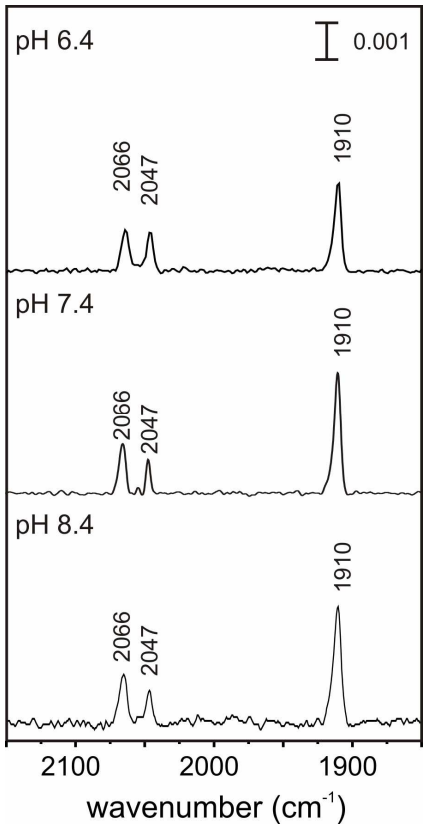

Potentiometric titrations.

The I_{NiB} , I_{NiSI}, I_{NiC}, I_{NiR} are the CO peak absorption intensities of the Ni-B, Ni-SI, Ni-C and Ni-R states, respectively.

The sum of these intensities at each applied potential equals:

$$I_{NiB} + I_{NiSI} + I_{NiC} + I_{NiR} = sum\,i \quad \text{(eq. 1)},$$

where i=1,…n the number of the respective potential step in the potentiometric titration. The individual normalized absorption peaks are given by:

$$\frac{I_{NiB}}{sum\,i} + \frac{I_{NiSI}}{sum\,i} + \frac{I_{NiC}}{sum\,i} + \frac{I_{NiR}}{sum\,i} = 1$$

$$I_{NiB}^{norm} + I_{NiSI}^{norm} + I_{NiC}^{norm} + I_{NiR}^{norm} = 1 \quad \text{(eq. 2)}$$

$E^{NiB/NiSI}$ is the reduction potential of the Ni-B/Ni-SI redox couple, E_{ap} is the applied electrode potential and $f = nF/RT$, where F is the Faraday constant (96485 C mol^{-1}), R is the universal gas constant (8.31447 J $K^{-1}mol^{-1}$) and T is the temperature (K) and n is the number of electrons that is taken equal to 1.

For the description of the ratios these relationships were used:

$$I_{NiB}^{norm} / I_{NiSI}^{norm} = exp(f(E_{ap} - E^{NiB/NiSI})) \quad \text{(eq. 3)}$$

$$I_{NiSI}^{norm} / I_{NiC}^{norm} = exp(f(E_{ap} - E^{NiSI/NiC})) \quad \text{(eq. 4)}$$

$$I_{NiC}^{norm} / I_{NiR}^{norm} = exp(f(E_{ap} - E^{NiC/NiR})) \quad \text{(eq. 5)}$$

Considering that $I_{NiB}^{norm} + I_{NiSI}^{norm} + I_{NiC}^{norm} + I_{NiR}^{norm} = 1$ (eq. 1) and solving with respect to the normalized peak absorption intensity of each redox state, we end up to the following equations that describe the behavior of each redox state as a function of the applied electrode potential that were used to fit the data in Figure 4 of the present manuscript:

$$I_{NiB}^{norm} = \frac{1}{1 + exp(-f(E_{ap} - E^{NiB/NiSI})) \cdot (1 + exp(-f(E_{ap} - E^{NiSI/NiC})) \cdot (1 + exp(-f(E_{ap} - E^{NiC/NiR}))))}$$

$$I_{NiSI}^{norm} = \frac{exp(-f(E_{ap} - E^{NiB/NiSI}))}{1 + exp(-f(E_{ap} - E^{NiB/NiSI})) \cdot (1 + exp(-f(E_{ap} - E^{NiSI/NiC})) \cdot (1 + exp(-f(E_{ap} - E^{NiC/NiR}))))}$$

$$I_{NiC}^{norm} = \frac{exp(-f(E_{ap} - E^{NiB/NiSI})) \cdot exp(-f(E_{ap} - E^{NiSI/NiC}))}{1 + exp(-f(E_{ap} - E^{NiB/NiSI})) \cdot (1 + exp(-f(E_{ap} - E^{NiSI/NiC})) \cdot (1 + exp(-f(E_{ap} - E^{NiC/NiR}))))}$$

$$I_{NiR}^{norm} = \frac{exp(-f(E_{ap} - E^{NiB/NiSI})) \cdot exp(-f(E_{ap} - E^{NiSI/NiC})) \cdot exp(-f(E_{ap} - E^{NiC/NiR}))}{1 + exp(-f(E_{ap} - E^{NiB/NiSI})) \cdot (1 + exp(-f(E_{ap} - E^{NiSI/NiC})) \cdot (1 + exp(-f(E_{ap} - E^{NiC/NiR}))))}$$

References

1. Fichtner, C.; Laurich, C.; Bothe, E.; Lubitz, W. *Biochemistry* **2006,** *45*, 9706

2. Bleijlevens, B.; van Broekhuizen, F. A.; De Lacey, A. L.; Roseboom, W.; Fernandez, V. M.; Albracht, S. P. J. *J. Biolog. Inorg. Chem.* **2004,** *9* , 743.

3. Saggu, M.; Zebger, I.; Ludwig, M.; Lenz, O.; Friedrich, B.; Hildebrandt, P.; Lendzian, F. *J. Biolog. Chem.* **2009,** *284* , 16264

4. Pandelia, Maria-Eirini. Doctoral Thesis, Technical University Berlin, Germany, 2009